Original Article

MOLECULAR METABOLISM

Semaphorin 4B is an ADAM17-cleaved adipokine that inhibits adipocyte differentiation and thermogenesis

Abdulbasit Amin [1,2], Marina Badenes [1,3,4], Johanna Tüshaus [5,6], Érika de Carvalho [1,7], Emma Burbridge [1,8], Pedro Faísca [1], Květa Trávníčková [9], André Barros [1], Stefania Carobbio [10,11], Pedro M. Domingos [7], Antonio Vidal-Puig [10,11], Luís F. Moita [1], Sarah Maguire [8], Kvido Stříšovský [9], Francisco J. Ortega [12,13,14], José Manuel Fernández-Real [12,13,14], Stefan F. Lichtenthaler [5,6,15], Colin Adrain [1,8,*]

ABSTRACT

Objective: The metalloprotease ADAM17 (also called TACE) plays fundamental roles in homeostasis by shedding key signaling molecules from the cell surface. Although its importance for the immune system and epithelial tissues is well-documented, little is known about the role of ADAM17 in metabolic homeostasis. The purpose of this study was to determine the impact of ADAM17 expression, specifically in adipose tissues, on metabolic homeostasis.

Methods: We used histopathology, molecular, proteomic, transcriptomic, *in vivo* integrative physiological and *ex vivo* biochemical approaches to determine the impact of adipose tissue-specific deletion of ADAM17 upon adipocyte and whole organism metabolic physiology.

Results: ADAM17$^{adipoq\text{-}cre\Delta/\Delta}$ mice exhibited a hypermetabolic phenotype characterized by elevated energy consumption and increased levels of adipocyte thermogenic gene expression. On a high fat diet, these mice were more thermogenic, while exhibiting elevated expression levels of genes associated with lipid oxidation and lipolysis. This hypermetabolic phenotype protected mutant mice from obesogenic challenge, limiting weight gain, hepatosteatosis and insulin resistance. Activation of beta-adrenoceptors by the neurotransmitter norepinephrine, a key regulator of adipocyte physiology, triggered the shedding of ADAM17 substrates, and regulated ADAM17 expression at the mRNA and protein levels, hence identifying a functional connection between thermogenic licensing and the regulation of ADAM17. Proteomic studies identified Semaphorin 4B (SEMA4B), as a novel ADAM17-shed adipokine, whose expression is regulated by physiological thermogenic cues, that acts to inhibit adipocyte differentiation and dampen thermogenic responses in adipocytes. Transcriptomic data showed that cleaved SEMA4B acts in an autocrine manner in brown adipocytes to repress the expression of genes involved in adipogenesis, thermogenesis, and lipid uptake, storage and catabolism.

Conclusions: Our findings identify a novel ADAM17-dependent axis, regulated by beta-adrenoceptors and mediated by the ADAM17-cleaved form of SEMA4B, that modulates energy balance in adipocytes by inhibiting adipocyte differentiation, thermogenesis and lipid catabolism.

Keywords ADAM17/TACE; Metabolism; Adipose tissue; Thermogenesis; Semaphorin4B Sema4b; Obesity; Cold challenge; Beta-adrenoceptor signalling

1. INTRODUCTION

Energy balance, the net outcome of caloric intake versus caloric expenditure, is controlled by complex communication amongst metabolic organs (e.g. brain, nervous system, adipose tissues, liver, pancreas, immune system and skeletal muscles) [1,2]. As a consequence of the rising obesity epidemic in developed and middle-income countries, extensive research efforts are dedicated towards identifying pathways that can be drugged to promote weight loss in obese subjects [3–5]. Adipose tissues are organs that play central roles in energy balance, organismal homeostasis and are implicated in a range of metabolic and infectious diseases [6–8]. They are specialized into 2 major functional classes: white adipose tissue (WAT) and brown adipose tissue (BAT). In the WATs, adipocytes store excess calories as

[1]Instituto Gulbenkian de Ciência (IGC), Oeiras, Portugal [2]Department of Physiology, Faculty of Basic Medical Sciences, University of Ilorin, Nigeria [3]Faculty of Veterinary Medicine, Lusofona University, Lisbon, Portugal [4]Faculty of Veterinary Nursing, Polytechnic Institute of Lusofonia, Lisbon, Portugal [5]German Center for Neurodegenerative Diseases (DZNE), Munich, Germany [6]Neuroproteomics, School of Medicine, Klinikum rechts der Isar, Technical University of Munich, 81675 Munich, Germany [7]Instituto de Tecnologia Química da Universidade Nova de Lisboa (ITQB-Nova), Oeiras, Portugal [8]Patrick G Johnston Centre for Cancer Research, Queen's University, Belfast, N. Ireland [9]Institute of Organic Chemistry and Biochemistry, Academy of Sciences of the Czech Republic, Prague, Czech Republic [10]Centro de Investigacíon Principe Felipe (CIPF), Valencia, Spain [11]Metabolic Research Laboratories, Institute of Metabolic Science, Addenbrooke's Hospital, University of Cambridge, UK [12]Girona Biomedical Research Institute (IDIBGI), Girona, Spain [13]Department of Medical Sciences, University of Girona, Girona, Spain [14]CIBER Fisiopatología de la Obesidad y Nutrición (CIBEROBN), and Institute of Salud Carlos III (ISCIII), Madrid, Spain [15]Munich Cluster for Systems Neurology (SyNergy), Munich, Germany

*Corresponding author. Patrick G Johnston Centre for Cancer Research, Queen's University Belfast, N. Ireland and Instituto Gulbenkian de Ciência (IGC), Oeiras, Portugal. E-mail: c.adrain@qub.ac.uk (C. Adrain).

Received October 11, 2022 • Revision received April 20, 2023 • Accepted April 21, 2023 • Available online 28 April 2023

https://doi.org/10.1016/j.molmet.2023.101731

triglycerides in a single lipid droplet comprising about 90% of cell volume. In the BAT, adipocytes contain multiple lipid droplets, are enriched in mitochondria and are highly catabolic [7]. One of the key ways in which adipocytes communicate, locally within an adipose tissue, or hormonally to distant target organs, is via secreted signaling molecules collectively known as adipokines. Prominent examples of adipokines include fibroblast growth factor 21 (FGF21), a protein that regulates hepatic gluconeogenesis, and enhances insulin sensitivity and thermogenesis in adipose tissue [6,9]. Another adipokine, the hormone leptin regulates energy balance centrally via the control of satiety [10,11]. Adipose tissues are themselves subject to incoming hormonal signals. They are richly innervated by sympathetic nerve endings that secrete the neurotransmitter norepinephrine (NE) in response to physiologic stimuli such as cold, overnutrition, and fasting [12—17]. WAT serves as reservoir of energy that can be mobilized when required (e.g. in the postprandial state, fasting, or during infection). The cue for energy release from WAT is signaled by NE, an activator of β-adrenergic receptors [17]. This triggers lipolysis in lipid droplets: the breakdown of triglycerides into their constituent free fatty acids (FFAs) and glycerol, which are released into the systemic circulation, to sustain energy-consuming organs [18—20]. Conversely, BAT converts the products of endogenous lipolysis (or exogenous lipolysis from WAT) into heat, via a process called non-shivering thermogenesis [21,22]. Upon β-adrenergic receptor activation by NE in brown adipocytes, a protein called uncoupling protein 1 (UCP1) is activated by free fatty acids [21]. Active UCP1 provides a channel through which protons generated by oxidative phosphorylation can leak across the inner mitochondrial membrane. The resultant futile cycle of proton movement, and the engagement of other unrelated futile biochemical cycles, generates heat [23,24].

Non-shivering thermogenesis contributes to the maintenance of a stable core body temperature under sub-thermoneutral conditions (e.g. lower than 30 °C in rodents). However, it also promotes energy balance in response to excessive caloric intake [21,25]. Notably, as the thermogenic activity of human BAT accounts for around 5% of total metabolic rate, steady-state energy consumption by BAT has been proposed to account for weight loss in the order of 4 kg/year [26]. A third class of thermogenic UCP1-expressing adipocytes, known as beige [27] (or brite [28]) adipocytes also exists. These adipocytes are interspersed within WAT and exhibit intermediate phenotypes between white and brown adipocytes [7,27]. In contrast to brown adipocytes which are specified during fetal development, beige adipocytes, which originate from distinct progenitors, can be recruited during adulthood [29]. This occurs via adipokine pathways and mechanisms that remain to be fully delineated, including trans-differentiation from white adipocytes. Another critical mechanism of beige adipocyte recruitment occurs via *de novo* adipogenesis, the differentiation of additional adipocytes from preadipocyte precursors, which is under the control of β-adrenoceptor signalling [29]. Adipogenesis also plays a key role in the *de novo* recruitment of white adipocytes, a process that has critical relevance for obesity (and is perturbed during ageing). The ability to recruit new white adipocytes to accommodate the increased lipid load associated with hypernutrition is key to mitigate the adverse effects associated with obesity [30]. Hence, it is increasingly recognized that it is metabolically more favourable to incur adipose tissue hyperplasia through *de novo* adipogenesis than to suffer hypertrophy of pre-existing adipocytes triggered by lipid overload, which can drive adipose tissue inflammation and insulin resistance [30]. Consequently, much research has been dedicated to elucidate the signalling molecules and mechanisms that predispose individuals towards the recruitment of beige adipocytes and/or the ability to mitigate the risk of adipocyte hypertrophy by driving *de novo* adipogenesis. Hence, pharmacological intervention to promote beiging or white adipose tissue hyperplasia by promoting adipogenesis is regarded as a potentially key intervention to improve metabolic health and promote weight loss [30—33]. The metalloprotease ADAM17 [34,35] is an important shedding protease ('sheddase') that cleaves some prominent signaling molecules. ADAM17 substrates include cell adhesion molecules, the ectodomains of TNF and its cognate receptors, TNFRI & TNFRII, some ligands of the epidermal growth factor receptor (EGFR) and gp130, the IL-6 co-receptor whose cleavage by ADAM17 mediates IL-6-*trans* signaling [36,37]. Consequently, ADAM17 is the key protease in regulating inflammation and growth. While numerous studies have dissected the role(s) of ADAM17 in inflammation and growth control, very few studies have focused on the role of ADAM17 in energy balance and obesity [38,39]. However, although deletion of ADAM17 results in perinatal lethality, a fraction of mice survives until adulthood in some studies [38]. These KO mice were reported to exhibit hypermetabolism that was not compensated by their elevated food intake, and so exhibited a lean phenotype [38]. Similarly, in another study, mice with a heterozygous deletion of ADAM17 were protected from obesity (by elevating their energy expenditure in response to high-fat diet) and its associated metabolic dysregulation, such as glucose intolerance and insulin insensitivity [39]. This evidence suggests that ADAM17 plays an important role as a repressor of energy expenditure, via the proteolysis of a yet unidentified substrate(s). Although a subset of the phenotypes (e.g. improved glucose tolerance and insulin sensitivity) in ADAM17 mutant mice can be attributed to impaired TNF cleavage [40,41], the equal susceptibility of these TNF-null mice to obesity compared to WT mice [42] shows that the negative impact of ADAM17 on energy expenditure cannot be attributed exclusively to TNF [40,41]. Hence, the proteolytic substrate(s) via which ADAM17 negatively regulates energy expenditure remain to be identified. Interestingly, the enhanced energy expenditure observed in ADAM17 mutant mice was associated with elevated levels of UCP1, implying that increased thermogenesis could underpin some of the observed hypermetabolic phenotypes [38]. In addition, we showed recently that mice null for inactive rhomboid 2 (iRhom2) are protected from diet-induced obesity [43]. Work from our group and others established that iRhom2 plays a crucial role in multiple aspects of ADAM17 biology including the control of its vesicular trafficking in the secretory pathway (which is coupled to the removal of its inhibitory prodomain) [44,45], its substrate specificity [46], and the activation of its activity on the cell surface by various stimuli [47,48]. In addition, an interactor called iTAP/FRMD8 is necessary to stabilize and maintain the function of the complex formed by iRhom2 and ADAM17 [49—51]. Notably, iRhom2-null mice also exhibit elevated energy expenditure and show increased thermogenesis (characterized by elevated BAT temperature) [43]. An early adaptation to an obesogenic dietary regime involves energy dissipation in the form of heat in BAT. This adaptation is driven by NE-mediated activation of β-adrenergic receptors. In the initial stage of adaptation, the sympathetic outflow to the adipose tissue is enhanced [52—54]. Therefore, the sympathetic nervous system (SNS) could impact on ADAM17 activity and the shedding of its substrates. Indeed, agonists of G protein-coupled receptors have been shown to induce the activation of other signaling pathways, such as the EGFR, via the stimulation of ADAM17 activity [55]. This process is known as receptor transactivation. Binding of agonists such as angiotensin II, lysophosphatidic acid (LPA), ATP, serotonin and endothelin-1 to their cognate GPCRs activates cell surface proteases such as ADAM17 to shed their substrates, which in turn activate other signaling pathways [56,57]. Here, we hypothesized that the GPCR agonist NE could activate

ADAM17 in adipocytes to shed substrate(s) that are important in the regulation of energy balance. We show that deletion of ADAM17 in adipocytes is sufficient to elevate energy expenditure under steady-state conditions and in obesity by increasing adipose tissue thermogenesis. This ameliorates overall organismal metabolic health in obese mice, by improving insulin sensitivity and glucose tolerance, dyslipidemia, and hepatosteatosis. Moreover, proteomic studies in primary adipocytes revealed that in response to β-adrenergic receptor activation by NE, ADAM17 catalyzes the shedding of the cell surface signaling protein, Semaphorin 4B (SEMA4B). Our work identifies SEMA4B as a novel adipokine whose ADAM17-dependent release from adipocytes, in response to sympathetic outflow, acts as a negative regulator of thermogenesis by downregulating genes associated with adipogenesis, and lipid synthesis and catabolism.

2. MATERIAL AND METHODS

2.1. Experimental animals

Mice were maintained in an SPF facility on a 12-hour light/dark cycle, at standard sub-thermoneutral conditions of 20−24 °C and an average of 50% humidity, in ventilated cages with corn cob as bedding. All mice were housed in this condition, except stated otherwise. Mice had access to food and water *ad libitum*. Male mice were fed with normal chow or high-fat diet (SNIFF diet D12492 60 kJ% fat, E15742: 60% of energy from fat). Animals were routinely co-housed to homogenize differences in microbiota and other environmental conditions. In the event where mice were housed in different cages, bedding material was interchanged between cages to facilitate normalization of the microbiota.

To generate adipocyte specific *Adam17* KO mice ($Adam17^{adipoq\Delta/\Delta}$), $Adam17^{fl/fl}$ (loxP site flanking exon2 [58]) (Jackson Laboratory, 009567) were crossed with $Adipoq^{Cre}$ mice [59]

All *in vivo* experiments were terminated by euthanizing mice with CO_2. Tissue samples were thereafter collected, snap frozen in liquid nitrogen for storage at −80 °C for future processing or fixed in appropriate fixatives until they were ready to be processed.

2.2. Study approval

Animal procedures were approved by the national regulatory agency (DGAV — Direção Geral de Alimentação e Veterinária) and by the Ethics Committee of Instituto Gulbenkian de Ciência and the Institutional Animal Care (A012.2016 and A001.2020), and were carried out in accordance with the Portuguese (Decreto-Lei no. 113/2013) and European (directive 2010/63/EU) legislation related to housing, husbandry, and animal welfare.

2.3. Cold shock and experiment at thermoneutrality

All mice were housed at the normal animal house ambient temperature of approximately 22 °C, from where these mice were exposed to the different experimental temperatures. Mice acclimatized to 30 °C were kept at this ambient temperature for 10 days, while those acclimatized to cold (4 °C) were kept at this temperature for 6h (short term exposure) or 10 days (longer term exposure).

2.4. Diet-induced obesity

To induce obesity, age-matched male mice were fed with high-fat diet (HFD, *SNIFF* diet D12492; 60 kJ% fat, 60% of energy from fat) for 26 weeks and were compared to control animals fed on standard chow. They were housed in large cages of 365 x 207 × 140 mm in dimension. These cages have the capacity to accommodate 16 mice. However, a maximum of 10 mice were housed per cage to guarantee enough space for the mice that develop obesity. Changes in mass of the mice were recorded weekly during the experiment.

2.5. Calorimetric measurements

The Promethion Core 8-cage system (Sable Systems) was used to assess body weight, food intake, energy expenditure (EE), locomotor activity (LA), and respiratory quotient (RQ) in mice fed on normal chow or HFD. Temperature was set at 22 °C for all experiments except where stated otherwise. For experiments in cold and thermoneutrality, temperatures were set as appropriate. Mice were acclimatised for at least 24 h in the metabolic cage system before the commencement of experiments.

2.6. Glucose and insulin tolerance tests

To test for glucose clearance or insulin sensitivity in the blood, mice exposed to normal chow or HFD for 22−24 weeks were fasted for 6 h (08:00−14:00). Fasting blood glucose was assessed by collecting blood from mice via tail puncture and using the one-touch Accu-Chek Aviva glucometer (Roche). Afterwards, mice were administered 1 g/kg of glucose (Fisher) intraperitonially to test glucose clearance or insulin (Humulin) in a dosage of 0.8 UI/Kg to chow-fed animals or 1 UI/Kg to HFD-fed mice to test insulin sensitivity. Subsequent changes in blood glucose were measured at 15, 30, 60 90, and 120 min post glucose or insulin administration. The area under the curve (AUC) was calculated using the trapezoid rule (the curve is divided into series of trapezoids and the sum of their area is the AUC).

2.7. Enzyme-linked immunosorbent assay (ELISA)

Blood was collected from 6 to 7 h fasted mice to quantify the concentration of insulin in the serum using an insulin ELISA kit (ALPCO). The medium of adipocytes was cleared and used to evaluate the levels of TNF, HB-EGF, Amphiregulin, and Sema4B using commercial ELISA kits (88-7324-22 eBioscience, DY8239-05, R&D Systems, DY989, R&D Systems, abx545290 ABBEXA B.V., respectively).

2.8. Serum lipid profile and liver lipid and function assessment

Serum from 6 to 7 h fasted mice were collected to quantify the levels of total cholesterol (TC), low density lipoprotein (LDLc), and triglycerides using enzymatic colorimetric kits (Spinreact). To quantify triglycerides (TG) in the liver, similar mass of liver was homogenized in a solution of chloroform and methanol (2:1). The homogenate was incubated overnight and centrifuged at 800 g for 15 min. The supernatant was subsequently mixed with 1/5 of its volume of saline solution (0.9% NaCl). The lower phase of the mixture was allowed to dry out after which a mixture of butanol/(Triton 100x/methanol) (2:1) was added for the colorimetric analysis of TG. To assess liver function, mouse serum samples were analyzed commercially (DNAtech) to evaluate the level of alanine transaminase (ALT) and aspartate transaminase (AST) in circulation.

2.9. Histopathology

Mice tissues such as liver, adipose tissues, muscle, and pancreas were collected and weighed. Tissues to be processed for histology were fixed in 4% formaldehyde. Liver samples intended for oil red staining were fixed in 4% formaldehyde for 24 h and thereafter transferred into 30% sucrose solution containing 0.005% NaN_3.

Adipose tissue (inguinal, epididymal, mesenteric, and retroperitoneal WAT, and BAT) and liver samples for H&E staining were embedded in paraffin, sectioned (3 μm per section) and stained with H&E. Adipocyte size was determined using a macro on the H&E-stained adipocyte images.

Adipose tissue inflammation (steatitis) was scored using the following classification: (0) no inflammation, (1) rare macrophage infiltration, (2) mild multifocal macrophage infiltration, (3) moderate multifocal macrophage infiltration, (4) severe multifocal macrophage infiltration. In the liver, steatosis was scored from 0 to 4, representing <5%, 5–33%, 34–66%, and >66% of the total area of the section affected, respectively.

For oil red staining in the liver, samples previously stored in 30% sucrose solution were snap-frozen and embedded in OCT. 8 μm of the tissues were cryosectioned and stained with oil red. Lipid content of the liver was scored as percentage of lipid per area of tissue. Adipocytes in culture were washed with PBS and fixed in 4% formaldehyde for at least 24 h and then stained with oil red. For the staining, samples were air-dried for 30 min, fixed in formalin for 5 min, and put under running water. Then, 5 dips into 60% isopropanol were performed and Oil Red O working solution (Oil red O, 00625, Sigma) was added for 15 min. Then, 15 dips into 60% isopropanol were performed and Mayer's Hematoxylin was added for 7 min. Samples were rinsed in 10x PBS, then in distilled water and afterwards mounted. The area of lipids was measured using the color threshold plugin of image J software. The fraction within the liver and the area per adipocyte nucleus was estimated.

Sections were examined and captured using a Leica DMLB2 microscope and Leica DFC320 camera, respectively. Whole slide images were acquired with Hammatsu Nanozoomer slide scanner and analysed in Fiji. Histopathological analysis was carried out by the in-house pathologist in a blinded manner.

2.10. Flow cytometry

Adipose tissue samples were digested in 1% collagenase H solution (Sigma) (1 h, 37 °C, with shaking). Spleens were mashed through a 70 μm cell strainer. The digested cells were centrifuged (5 min, 4 °C, 2000 rpm), and red blood lysis buffer was added (9 vol. NH4Cl and 1 vol. Tris-Cl). The cells were washed and filtered through a 70 μm strainer. Cells were incubated in Fc Block, clone 2.4G2 (1:100, produced in-house) and staining was then performed with anti-mouse CD45.2-PE (1:100, produced in-house), CD11b-FITC (1:100; produced in-house), F4/80-PE-Cy7 (1:100; 123114; Biolegend), CD11c-PerCP (1:100, produced in-house), CD206-BV421 (1:100; 141717; Biolegend), Ly6C-APC-Cy7 (1:100; produced in-house), Zombie viability dye (1:1000; 423113; Thermo Fisher Scientific) and incubated for 20 min at 4 °C. The cells were afterwards wash in FACs buffer (1x PBS containing 2% calf serum) and centrifuged at 300 g for 5 min at 4 °C. Cell pellets were resuspended in FACs buffer and analysed in the LSRFortessa X-20 with FlowJo software, version 10.2.

2.11. Thermography

To measure BAT temperature, mice were anaesthetized using isoflurane. The fur covering the scapular and interscapular dermal surface was shaved. Mice were then allowed to recover by housing them individually in cages for 24 h with free access to food and water *ad libitum*. Food was withdrawn 2 h before thermal images of the interscapular region of the mice were captured using a thermal camera (FLIR). Resulting images were analyzed in the FLIR image software. Rectal temperature was measured using a rodent thermometer (Bioseb).

2.12. Mouse primary adipocyte culture

The inguinal white adipose tissue (iWAT) and interscapular BAT (iBAT) were collected from 4–5-week-old male or female C57Bl/6, *Adam17*$^{fl/fl}$, or *Adam17*$^{adipoq\Delta/\Delta}$ mice for primary inguinal and brown adipocyte cultures, respectively. A culture was made from a pool of 3–5 mice. The tissues were cleaned, minced, and transferred into a 50 ml falcon. Two ml of Hank's balanced salt solution (Biowest) supplemented with 1 mg/ml collagenase (Fisher Bioreagents), 10 mM $CaCl_2$ (Sigma), and 2.2 mg/ml dispase II (Roche) was added to the minced tissue and put to shake at 37 °C for 30–45 min. DMEMF12 (Biowest) was added to the mixture to stop digestion. The resultant solution was passed through 100 μm cell strainer. The filtrate was centrifuged at 500 g for 10 min at 4 °C. The pellet was resuspended again in DMEMF12 and filtered through 40 μm cell strainer. The resultant filtrate was again centrifuged at 500 g for 5 min at 4 °C. The resultant pellet was resuspended in complete medium (DMEMF12 supplemented with 1% penicillin-streptomycin solution 100X, 2.5 μg/ml amphotericin B (Life Tech), 10 μg/ml gentamycin sulphate (Sigma), and 10% new-born calf serum (Biowest)), plated in 10 cm dish and incubated at 37 °C, and 5% CO_2. At confluence, preadipocytes were plated in collagen I (Corning) coated 6 or 12 well plates at 500,000, or 200,000 cells per well. respectively, to reach confluence. Differentiation was induced by exposing confluent cells to differentiation medium (complete medium supplemented with 1 mM 3-isobutyl methylxanthine (AppliChem), 2 μM rosiglitazone (Cayman), 10 μM dexamethasone (Cayman), 1 μg/ml insulin (Sigma), and 2 nM 3,3′,5-Triiodo-L-thyronine (Sigma)) on day 0 and day 2. On day 4 and day 6 post induction, differentiating cells were exposed to maintenance medium (complete medium supplemented with 1 μg/ml insulin (Sigma), and 2 nM 3,3′,5-Triiodo-L-thyronine (Sigma)). On day 8 post induction, the cells were used for relevant experiments.

2.13. Assessment of thermogenic gene expression in adipocyte cultures

Fully differentiated primary adipocytes were washed with serum free medium (SFM) (DMEMF12 supplemented with 1% penicillin-streptomycin solution 100X, 2.5 μg/ml amphotericin B (Life Tech), and 10 μg/ml gentamycin sulphate (Sigma)). SFM was replaced with SFM containing 2% bovine serum albumin (BSA) (Merck). To stimulate the βARs, the cells were treated with 2 μM norepinephrine (NE) (Sigma). The cells and/or medium were collected at specific time points depending on the experiment.

For the experiment showing increased shedding of TNF, HB-EGF, Amphiregulin, and Sema4B upon βAR stimulation, fully differentiated WT and ADAM17 KO primary adipocytes were treated with NE for 1 h for the first three and for 10 h for Sema4B. ADAM17 inhibitor BB94 (196440, Calbiochem) at 10 μM was added 1h prior NE for the Sema4B assessment. For experiments aimed at assessing the regulation of thermogenic genes in WT and ADAM17 KO primary adipocytes fully differentiated cells were treated with NE for 6 h, while cells intended for assessing protein expression were treated with NE for 3 h, 6 h, 12 h, and 24 h, depending on the specificities of the experiment.

2.14. Assessment of lipolysis in adipocyte cultures

Serum free medium with or without NE was added to differentiated immortalized brown adipocytes overexpressing the cleaved version of Sema4B versus controls. The medium was collected each 15 min for a period of 1 h to assess the glycerol (F6428, Sigma) content. Cells were washed three times and starved for 1 h prior the experiment.

2.15. Quantitative transcriptional analysis

Adipose tissues (iBAT, iWAT, and epididymal WAT), liver, and primary adipocytes collected at the end of experiments for transcriptional

analysis were snap frozen and lysed in NR buffer of the NZYTech total RNA extraction kit. Subsequent steps for collection and purification of RNA were guided by the protocol of the kit. First-strand cDNA was synthesized from RNA using the Xpert cDNA synthesis master mix (GRiSP). SYBR green or Taqman reagents (GRiSP) were used for real time PCR. The comparative C_T method was employed and GAPDH and Actin were used in normalizing gene expression. In the case of human fat samples, total RNA was extracted using the RNeasy Mini Kit (QIAgen, 74104). 3 μg were retro-transcribed into cDNA using the High Capacity cDNA Archive Kit (Applied Biosystems, 4368814). Commercially available SYBR Green I, with forward/reverse paired primers (KiCqStart® SYBR® Green Primers; Sigma, KSPQ12012), were used to assess the expression of gene candidates in a Light Cycler 480 II sequence detection system (Roche Diagnostics). The gene expression levels were normalized to the respective reference gene transcript, which was human cyclophilin A (PPIA). The normalized fold expression was obtained using the $2^{-\Delta\Delta Ct}$ method. Replicates and positive and negative controls were included in all reactions. The primer sequences for qPCR and Taqman probes used are listed below (Table 1).

2.16. Evaluation of expression of Sema4B and its receptors in human tissues

The data in Supplementary Figs. 6A and B were replotted from publicly available data. The data in Supplementary Fig. 6A were replotted from data from an experiment in which two human pluripotent stem cell lines (H9 and KOLF2-C1) were differentiated into brown adipocytes [60]. The data in Supplementary Fig. 6B were obtained from a study in which human adipocytes were differentiated from SVF obtained from subcutaneous WAT and subclavicular BAT from human subjects [61].

Table 1 — List of primers and Taqman probes.

Gene		Taqman probe ID
Adam17		Mm00456428_m1
Actin		Mm00607939_s1
ADAM17		Hs01041915_m1
RHBDF2		Hs00226277_m1
Gene	**SYBR, Forward primer (5′-3′)**	**SYBR, Reverse primer (5′-3′)**
Actin	AGGGAAATCGTGCGTGACAT	GAACCGCTCGTTGCCAATAG
Gapdh	AACTTTGGCATTGTGGAAGG	ACACATTGGGGGTAGGAACA
Ucp1	ACTGCCACACCTCCAGTCATT	CTTTGCCTCACTCAGGATTGG
Pgc1α	CCCTGCCATTGTTAAGAC	TGCTGCTGTTCCTGTTTTC
Prmd16	CAGCACGGTGAAGCCATT	GCGTGCATCCGCTTGTG
Dio2	CAGTGTGGTGCACGTCTCCAATC	TGAACCAAAGTTGACCACCAG
Cox8b	GAACCATGAAGCCAACGACT	GCGAAGTTCACAGTGGTTCC
Cidea	TGCTCTTCTGTATCGCCCAGT	GCCGTGTTAAGGAATCTGCTG
Atgl	TGGTTCAGTAGGCCATTCCT	CACTTTAGCTCCAACCATGA
Hsl	TGCTCTTCTTCGAGGGTGAT	TCTCGTTGCGTTTGTAGTGC
Adipoq	GCACTGGCAAGTTCTACTGCAA	GTAGGTGAAGAGAACGGCCTTGT
C/ebpα	AAACAACGCAACGTGGAGAC	TGTCCAGTTCACGGCTCAG
Pparγ	ATTCTGGCCCACCAACTTCGG	TGGAAGCCTGATGCTTTATCCCCA
PPARα	AGAGCCCCATCTGTCCTCTC	ACTGGTAGTCTGCAAAACCAAA
Fasn	AAGGCTGGGCTCTATGGATT	GGAGTGAGGCTGGGTTGATA
Dgat	CCGCAAAGGCTTTGTGAA	GGAATAAGTGGGAACCAGATCAG
Scd1	CTGACCTGAAAGCCGAGAAG	GCGTTGAGCACCAGAGTGTA
Apoe	GCTGGGTGCAGACGCTTT	TGCCGTCAGTTCTTGTGTGACT
Apob	CGTGGGCTCCAGCATTCTA	TCACCAGTCATTTCTGCCTTTG
Mcad	TGGAGACATTGCCAATCAGC	ACCATAGAGCTGAAGACAGG
Aco	AAGAGTTCATTCTCAACAGCC C	CTTGGACAGACTCTGAGCTGC
TNF	ATGAGCACAGA AAGCATGATC	TACAGGCTTGTCACTCGAATT
Il6	ACGGCCTTCCCTACTTCACA	CATTTCCACGATTTCCCAGA
Il1β	GAAGAAGAGCCCATCCTCTG	TCATCTCGGAGCCTGTAGTG
MCP1	GGAAAAATGGATCCACACCTTGC	TCTCTTCCTCCACCATGCAG
PLXNB1	GTCTGTATACCTTCGTGAGG	TGTCGTTCAAGGTGTATTTG
PLXNB2	AGGAGAAGATCATTGACCAG	CATTGTAGTGCATAAGGGTG
NRP1	AGAAGATTGTGCAAAACCAG	TAAGGTCTTCAACACATTGC
NRP2	AGGTATTTCAAGCCAACAAC	CGGATTCTAACAAACCTTGTC
SEMA4B	TTCTATGGGGTCTTCACTTC	CCTTCATTGTGAAGACACAG
PPIA	CTCCACAATATTCATGCCTTC	ATGGTTCCCAGTTTTTCATC

2.17. Western blotting

Mouse adipose tissues and primary adipocytes samples were lysed in lysis buffer (1% Triton X-100, 150 mM NaCl, 50 mM Tris—HCl, pH 7.4) supplemented with protease inhibitors and 10 mM 1,10 phenanthroline. To improve the detection of ADAM17, homogenates were incubated overnight in concanavalin A resin at 4 °C. The incubated homogenates were then centrifuged at 1000 g for 2 min at 4 °C. The pellets (resin) were washed in lysis buffer (supplemented with protease inhibitors and 10 mM 1,10 phenanthroline) 3 times. The beads were eluted in sample buffer supplemented with 15% sucrose by heating at 65 °C for 15 min. When homogenates were not enriched to improve the detection of specific proteins, equal amount of protein from different samples were denatured in sample buffer by heating at 65 °C for 15 min. In some cases, the denatured lysates were digested for 2 h at 37 °C with the deglycosylating enzyme PNGase F, which removes high mannose N-linked glycans added in the ER and complex N-linked glycans found in the later secretory pathway. Then, the samples were denatured for 15 min at 65 °C. The samples were fractionated in SDS-PAGE before being transferred onto PVDF membrane. The membranes were blocked in Tris-buffered saline with 0.1% Tween® 20 Detergent (TBS-T) supplemented with 5% milk or BSA for at least 30 min and then incubated in primary antibodies (diluted in TBS-T supplemented with 5% milk or BSA) overnight at 4 °C. The following primary antibodies were used: rabbit anti-ADAM17 antibody (1:1000, Ab39162, Abcam), mouse anti-Flag HRP (1:1000; A8592; Sigma), mouse anti-Transferrin receptor (1:1000, 13—6800, Life Technologies), rat anti-tubulin (1:1000 Clone YL1/2, IGC antibody facility), rabbit anti-ATGL (1:500; 2138, Cell Signaling), rabbit anti-pHSL (1:500; Ab109400, Abcam), mouse anti-p97 ATPase (1:1000, 65278, Progen). The membranes were subsequently washed 4 times in TBS-T for 10 min before incubating in the appropriate secondary antibody anti-rabbit HRP (1:5000; 1677074P2, Cell Signaling Technology) or anti-mouse HRP (1:5000; 1677076P2, Cell Signaling Technology) diluted in TBS-T supplemented with 5% milk or BSA for at least 30 min. The membranes were again washed 4 times in TBS-T for 10 min followed by a 10 min wash in Phosphate buffer saline (PBS). Protein bands were detected using ECL. Images were captured using the Amersham™ imager 600.

2.18. Primary adipocyte secretome analysis with high-performance secretome protein enrichment with click sugars (hiSPECS)

To analyze the secretome from *Adam17*$^{fl/fl}$ and Adam17$^{Adipoq/}$ primary adipocytes, maintenance medium was added to differentiated adipocytes on day 6 post-induction of differentiation (300,000 preadipocytes were plated per well of a 6-well plate before the induction of differentiation) was supplemented with 50 μM of ManAZ (Thermo Fisher Scientific, Cat #C33366) for 48h. The conditioned medium from these cells was collected to analyze the secretome of the primary adipocytes in steady state. However, to assess the changes in the secretome upon induction of thermogenesis, the 48 h-long maintenance medium supplemented with 50 μM of ManNAz was replaced with SFM supplemented with 10% serum and 50 μM of ManNAz for 12 h. The cells were stimulated, or not, with 2 μM of norepinephrine during this period. 1 ml of the medium from the cells were collected and filtered through a 0.45 μm centrifuge tube filter (Costar® Spin-X #10649351). Proteinase inhibitor (1:500) was added to the filtrate and the samples

were stored at −20 °C until further use. The hiSPECS workflow, as previous described in detail [62] was performed. In brief, glycoproteins were enriched using Concanavalin A and azido-modified proteins were immobilized on magnetic DBCO-beads (Jena Bioscience #CLK-1037-1) via click chemistry. Stringent washing steps reduced contaminants and peptides were released from the beads by tryptic digest. Desalted peptides were analyzed using liquid chromatography mass spectrometry (LC-MS/MS) using an EASY-nLC 1200 UHPLC system (Thermo Fisher Scientific) coupled to an Q Exactive HF mass spectrometer (Thermo Fisher Scientific). Data-dependent acquisition (DDA) and data-independent acquisition (DIA) analysis was applied and data analysis was performed with MaxQuant and Spectronaut. Proteins were considered sufficiently expressed if detectable in at least 4 of the 5 samples per treatment condition. To enrich for candidate membrane proteins shed by metalloprotease activity we focused on proteins that have a single transmembrane helix (TM1), two transmembrane helices (TM2), or a glycosylphosphatidylinositol (GPI) anchor, as previously described [63]. A p-value $\leq$0.05 was used as cut-off for significantly and differentially shed proteins.

2.19. Assessment of Sema4B cleavage in cultured cells

Wild type and ADAM17 KO HEK293ET cells were kind donations from the Becker-Pauly Lab, University of Kiel, Germany. Full length flag-tagged Sema4B plasmid was donated by the Püschel Lab, University of Munster, Germany [64]. To test for the potential shedding of Sema4B ectodomain by ADAM17, Wild type and ADAM17 KO HEK293 cells were plated overnight in a 6-well plate (500,000 cells per well). The day after, the cells were transfected with Sema4B or an empty vector using Polyethyleneimine (PEI). In brief, cells plated overnight had their medium changed for 2 ml of complete medium containing 2.5 μg of Sema4B plasmid DNA or empty vector and 7.5 μg of PEI per well. Twenty-four hours after transfection, the medium of the cells was aspirated, the cells were washed with SFM, and serum-starved for 4 h. Thereafter, cells were treated with vehicle or phorbol-12-myristate-13-acetate (PMA) for 1 h to stimulate ADAM17 activity. The media were collected to precipitate protein content and the cells were lysed to be processed for western blot as previously described [65].

2.20. Lentiviral transduction

HEK293 ET packaging cells (6×10^6) were transfected with pCL-Eco packaging plasmid [66] plus SV40 Large T Ag, or (16.6×10^6) with the pMD-VSVG envelope plasmid, psPAX2 helper plasmid plus pLEX, or pLEX containing mouse truncated Semaphorin 4B cDNA fused to a Flag tag. The packaging vectors for the production of lentivirus were described previously [67]. WT brown preadipocytes from a WT newborn mouse was immortalized as previously described [68]. In summary, isolated cells were split in two and seeded in a 35-mm plate at 40% confluence and one well was transduced with 2 ml of SV-40 supernatant supplemented with polybrene 8 μg/ml twice with a 24h interval. The non-transduced cells were used as control. Then, the immortalized cells were transduced with 20 μl of 150x ultracentrifuged (90,000 g, 4 h, at 4 °C) empty vector (pLex), Semaphorin 4B viral supernatant (resuspended in 0.1% BSA in PBS) supplemented with polybrene 8 μg/ml, and selected with puromycin (10 μg/ml) for 2 days to generate stable cell lines. These cells were differentiated using the standard protocol.

2.21. Expression and purification of Semaphorin 4B ectodomain

Expi293F cells (Thermo Fisher Scientific) were cultured in Expi293 Expression Medium and transfected with the pCMVi-SV40 ori-based plasmid encoding amino acids 1 to 700 of mouse Semaphorin 4B (Uniprot ID Q62179) followed by PreScission cleavage site, hexahistidine tag and Twin Strep tag. Five days after transfection, medium with secreted ectodomain of Sema4B was collected, and flash frozen in liquid nitrogen. For purification of Sema4B ectodomain, the thawed medium was loaded onto Strep-Tactin® Superflow® high capacity cartridge (IBA Lifesciences GmbH) pre-equilibrated in the binding buffer (100 mM Tris—HCl pH 8.0, 150 mM NaCl). Unbound material was washed away with 10 column volumes of binding buffer, and Sema4B ectodomain was eluted with 5 column volumes of the elution buffer (100 mM Tris—HCl pH 8.0, 150 mM NaCl, 2.5 mM desthiobiotin). Glycerol was added to the purified protein to 10% (v/v) before flash freezing it in liquid nitrogen. Finally, purified Sema4B ectodomain was depleted from any possible traces of endotoxins by the Pierce™ High Capacity Endotoxin Removal Spin Column (Thermo Fisher Scientific), according to the manufacturer's protocol. The final preparation of Sema4B ectodomain was flash frozen in small aliquots in liquid nitrogen and stored at −80 °C for further use.

2.22. RNA sequencing and data analysis

Immortalized murine brown adipocytes stably transduced with lentiviruses harboring pLEX empty vector or a mimetic of the ADAM17-cleaved form of Sema4B (described above, 2.19) were plated at a density of 300,000 cells/well in 6-well plates. The following day, after achieving confluence, the cells were differentiated to matured adipocytes over a period of 8 days as described above (2.12). Medium from matured adipocytes was aspirated and the cells were washed with serum-free medium (SFM). Afterwards, the cells were incubated in SFM supplemented with 2% BSA with or without 2 μM NE for 6 h. At the end of this timepoint, the cells were washed with cold PBS and the cells were lysed using the NR buffer of the NZYTech total RNA extraction kit. Subsequent steps for collection and purification of RNA were guided by the protocol of the kit. For the RNA sequencing, full-length cDNAs were generated following the SMART-Seq2 protocol described by Picelli et al., 2014 [69]. After quality control using Fragment Analyzer (Agilent Technologies), library preparation including cDNA fragmentation, PCR-mediated adaptor addition and amplification of the adapted libraries was done following the Nextera library preparation protocol (Nextera XT DNA Library Preparation kit, Illumina), as previously described [70]. Libraries were confirmed by Fragment Analyzer (Agilent Technologies) and then sequenced (NextSeq2000, Illumina) using 100 SE P2. Sequence information was extracted in FastQ format, using Illumina DRAGEN FASTQ Generation v3.8.4. Library preparation and sequencing were optimized and performed by Genomics Unit at the Instituto Gulbenkian Ciência. Raw fastq reads were processed using FastQ Screen to identify any non-murine reads prior to alignment. Reads passing were aligned to the mouse genome (mm10, GRCm38.p4) using STAR v2.7.9a [71]. Counts per gene were calculated using htseq-count [72]. Differential gene expression analysis was performed with DESeq 2 [73], with an adjusted p-value cut-off of $\leq$0.05 and a foldchange cut-off of $\geq$1. RNAseq data have been uploaded to NCBI GEO (GSE228157). Pathway enrichment was performed with DAVID [74]. Normalized gene counts were log2-scaled and z-scored for data visualization. Heatmaps were generated in the R statistical programming language (https://cran.r-project.org/).

2.23. Human data analysis

Samples of subcutaneous (SC) and paired (n = 89) and unpaired visceral adipose tissue (VAT) were obtained from the same region (lateral to the umbilicus) and studied in cohort 1.Cohort 1 consisted of 181 individuals (42% men) with body mass indexes (BMI) ranking between 18 and 60 kg/m2. BMI was calculated by dividing weight in

Table 2 — Anthropometric and biochemical parameters of obese (BMI≥30 kg/m^2, n = 105) and non-obese (BMI<30 kg/m^2, n = 76) subjects in cohort 1.

	BMI<30	Obesity	*p*-value[a]
n (men/women)	34/42	42/63	
Age (years)	51 ± 10	46 ± 11	**0.001**
Body Mass Index (kg/m^2)	25.3 ± 3.6	43.9 ± 7.0	**<0.0001**
Fat mass (%)	34.1 ± 7.2	55.7 ± 9.6	**<0.0001**
SBP (mmHg)	124.8 ± 16.7	135.0 ± 17.0	**<0.0001**
DBP (mmHg)	73.9 ± 13.0	79.2 ± 11.0	**0.007**
Fasting glucose (mg/dl)	93.2 ± 18.2	104.6 ± 38.9	**0.01**
Hb1Ac (%)	5.6 ± 1.3	5.4 ± 1.1	0.244
Cholesterol (mg/dl)	187.7 ± 32.1	203.7 ± 42.6	**0.005**
HDL (mg/dl)	63.2 ± 22.2	54.6 ± 15.9	**0.006**
LDL (mg/dl)	109.7 ± 28.2	121.0 ± 34.6	**0.024**
Triglycerides (mg/dl)	103.5 ± 54.7	118.8 ± 77.9	0.154

Values represent the mean ± standard deviation. **S/DBP**: systolic/diastolic blood pressure; **Hb1Ac**: glycated haemoglobin; **H/LDL**: high/low density lipids; [a]Student t-test for non-obese subjects vs. obese participants. **Bold** indicates significant results (p-value <0.05).

kilograms by the square of the height in meters (Kg/m2), and obesity was set up at BMI>30 kg/m2. Subjects' characteristics are provided in Table 2. Samples of subcutaneous (SC) and paired (n = 89) and unpaired visceral adipose tissue (VAT) were obtained from the same region (lateral to the umbilicus) and studied in cohort 1. Cohort 2 included 23 morbidly obese women followed for an average of ~2 years after bariatric surgery. Samples of SC adipose tissue were retrieved at the baseline and follow up, as described elsewhere [75]. The characteristics of individuals from cohort 2 are provided in Table 3. All participating subjects were of Caucasian origin, gave written informed consent, and reported that their body weight had been stable for at least three months before entering the study. Samples and data from participants of this study were given by the FATBANK platform, promoted by the CIBEROBN, and coordinated by the IDIBGI Biobank (Biobanc IDIBGI, B.0000872). All samples were processed following standard operating procedures, with the appropriate approval of the Ethics, External Scientific and FATBANK Internal Scientific Committees. To confirm the regulation of our current gene candidates in bulk adipose tissue, microarray gene expression measurements were retrieved from the study of Kerr et al. [97]. There, biopsies of SC adipose tissue were obtained by needle aspiration from 50 obese women at the baseline and 2 (n = 49) and 5 (n = 38) years after being gastric bypassed, and also from a non-operated group of 28 healthy weight women matched for age.

Table 3 — Spearman rank correlation between omental (VAT) and subcutaneous (SAT) gene expression and BMI from Cohort 1 (see Table 2).

	VAT BMI (kg/m^2)			SAT BMI (kg/m^2)		
	Rho	Sig. (bilateral)	N	Rho	Sig. (bilateral)	N
TNFα	0.456	**8.486E-09**	145	0.374	**2.777E-07**	178
iRHOM2	0.235	**0.027**	88	0.269	**0.001**	145
ADAM17	0.074	0.494	88	0.257	**0.002**	145
SEMA4B	0.101	0.237	138	−0.071	0.455	113
PLXNB1	0.130	0.128	138	−0.071	0.463	112
PLXNB2	0.248	**0.003**	138	0.026	0.787	112
NRP1	−0.162	0.058	138	0.064	0.502	112
NRP2	0.178	**0.038**	137	0.104	0.276	112

2.24. Statistical analysis

Statistical analyses carried out were performed using R (https://www.r-project.org), SPSS (IBM Analytics) and/or GraphPad Prism 6 software. All data are expressed as mean ± S.D.. Statistical significance was determined by Student's or paired t test (when two groups were compared), or by one-way analysis of variance ANOVA (when more than two groups were compared) followed by post hoc Bonferroni test. The relation between variables was analysed by Spearman's rank correlation test and multiple regressions analyses, when necessary. A p-value <0.05 was considered as statistically significant.

3. RESULTS

3.1. Beta-adrenergic receptor activation stimulates ADAM17 to repress thermogenesis in adipocytes

Our previous study established that mice null for iRhom2, the key regulator of ADAM17 trafficking and activity [44,45] exhibit elevated adipose tissue thermogenesis and Ucp1 levels [43]. As noted above, a fraction of ADAM17 KO mice that escape embryonic lethality and survive into adulthood also exhibit elevated Ucp1 levels [38]. Together, this evidence led us to hypothesize that ADAM17 acts within adipose tissue to repress thermogenic signals. To test this hypothesis, we generated mice in which ADAM17 was deleted in adipocytes using adiponectin-cre (adipoq-cre) [59] (Fig. S1A). ADAM17 activity can be activated by certain classes of G protein-coupled receptors (GPCR) [76,77]. As adipocyte beta adrenergic receptors (βARs) control thermogenic responses and lipolysis [78], we tested the hypothesis that the endogenous βAR agonist norepinephrine (NE) can transactivate pathways mediated by substrates of ADAM17. Hence, we isolated adipocyte progenitors from the stromal vascular fraction (SVF) from inguinal adipose tissues of control floxed (ADAM17 $^{fl/fl}$) versus *Adam17*$^{adipoq\Delta/\Delta}$ mice in which ADAM17 was deleted in adipocytes (henceforth referred to as "WT" and "KO" throughout) and differentiated them to mature adipocytes *ex vivo*. As shown in Fig. S1A, a significant decrease was observed in the protein levels of ADAM17 in adipocytes differentiated from SVF obtained from the KO mice relative to the WTs. Focusing on iWAT, a tissue that is susceptible to beiging [27], mature primary adipocytes were stimulated with NE and the shedding of several crucial ADAM17 substrates (TNF (Tumor necrosis factor); HB-EGF (Heparin-binding EGF); and AREG (Amphiregulin)) into the culture media was quantified by ELISA. Notably, NE stimulation significantly increased the shedding of TNF, HBEGF, and AREG in WT adipocytes, while shedding of these substrates was inhibited in the ADAM17 KO adipocytes (Figure 1A). These data show that activation of endogenous βARs triggers a cascade of events that stimulate the proteolysis of ADAM17 substrates and links ADAM17 regulation to a critical pathway that governs adipocyte physiology. In addition to the stimulatory effects of NE in promoting the shedding of some ADAM17 substrates, we also observed that βAR activation also impacted the levels of ADAM17. As shown in Figure 1B, stimulation of WT mature primary inguinal adipocytes with NE over a 24-hour period revealed a complex impact of βAR activation on ADAM17. At 3 h post-stimulation, βAR activation triggered an increase in the overall levels of ADAM17, particularly in the levels of the mature form of the protease that has reduced molecular weight (Fig. 1B). At later timepoints, the levels of ADAM17 decreased over time becoming almost non-detectable 12 h post-stimulation with NE, after which, a gradual recovery in ADAM17 levels was observed 24 h post induction with NE (Fig. 1B). βAR activation also elevated *Adam17* mRNA levels by approximately 2-fold in primary inguinal WT adipocytes (Fig. 1C). To test the impact of these observations in an *in vivo* setting, we modulated sympathetic neuron

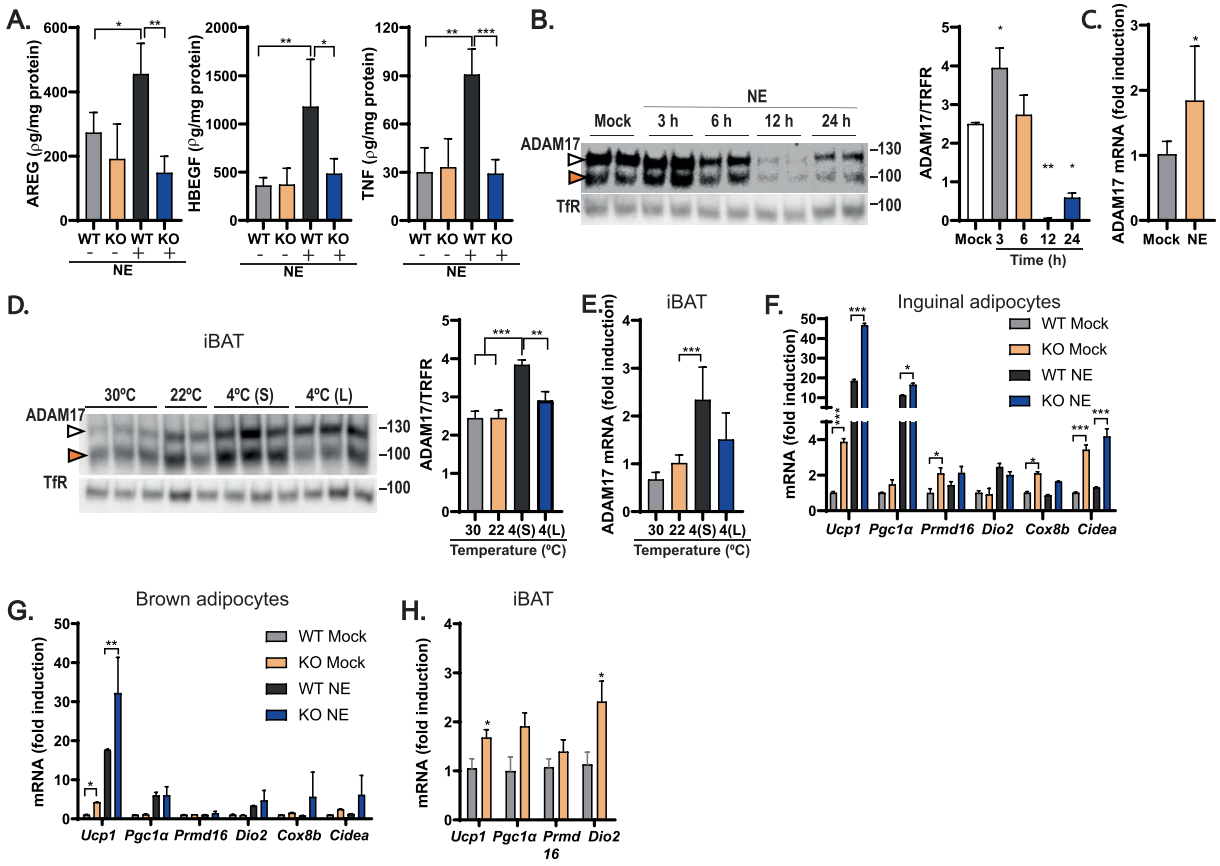

Figure 1: Loss of ADAM17 in adipocytes increases thermogenesis in primary adipocytes and elevates energy expenditure *in vivo*. **(A)**, Amphiregulin (AREG), heparin-binding growth factor (HB-EGF), and tumor necrosis factor (TNF) levels quantified by ELISA in conditioned media from control and ADAM17 KO primary adipocytes with or without stimulation for 1 h with 2 μM of norepinephrine (NE) (n = 4). **(B)**, Immunoblots showing mature (100 KDa) (orange arrowhead) and immature (130 KDa) (white arrowhead) ADAM17 from untreated WT primary adipocytes and primary adipocytes stimulated with 2 μM of NE over different time points for a total period of 24 h. Total ADAM17 (matured and immature ADAM17) quantified as a ratio of the loading control, transferrin receptor (TfR) (n = 4). **(C)**, mRNA levels of *Adam17* in WT primary adipocytes without or with treatment with 2 μM of NE (n = 4). **(D)**, Immunoblot showing mature (100 KDa) (white arrowhead) and immature (130 KDa) (orange arrowhead) ADAM17 levels in interscapular brown (iBAT) in WT mice exposed to different ambient temperatures; thermoneutrality (30 °C for 10 days), standard animal house temperature (22 °C), acute cold exposure (4° S; 4 °C for 6 h), and chronic cold exposure (4° L; 4 °C for 10 days). Total ADAM17 (mature and immature ADAM17) quantified as a ratio of the loading control, transferrin receptor (TfR) (n = 6 all conditions except n = 4 for 22 °C). **(E)**, mRNA levels of *Adam17* in the iBAT of mice from D (n = 6). **(F&G)**, mRNA level of positive regulators of thermogenesis in control and ADAM17 KO primary inguinal (**F**) and brown (**G**) adipocytes treated without or with 2 μM of NE (n = 4). **(H)**, mRNA level of the thermogenic genes, *Ucp1, Pgc1α, Prmd16*, and *Dio2* in the iBAT of lean control (WT) and adipocyte-specific ADAM17 KO (KO) mice (n = 5). Results presented as mean ± SD. *P < 0.05, **P < 0.01, ***P < 0.001, ****P < 0.0001. (For interpretation of the references to color in this figure legend, the reader is referred to the Web version of this article.)

output and hence NE release and βAR activation by exposing WT mice to different ambient temperatures. Mice were either acclimated to thermoneutrality (30 °C, to minimize sympathetic output), room temperature (22 °C), or cold (4 °C, to enhance sympathetic output) after which interscapular brown adipose tissues were isolated. As shown in Figure 1D,E, exposure of WT mice to acute cold increased the protein and mRNA expression levels of ADAM17 in brown adipose tissue, but not in iWAT (Figure S1B and C). Taken together with the primary adipocyte data (Figure 1A–C), this suggests that, in response to sympathetic output and βAR activation, ADAM17 could play a role in the physiological adaptation of the BAT to decreasing ambient temperature. To understand the impact of ADAM17 on thermogenesis, we quantified the level of expression of thermogenic genes in primary inguinal and brown adipocytes differentiated from the SVF of WT versus KO mice. Notably, loss of ADAM17 in adipocytes upregulated the expression of some thermogenic genes in inguinal and brown adipocytes, both under basal conditions and in response to NE (Figure 1F,G). In addition, we found there was a trend (*p*-value = 0.0858) towards increased adipogenesis in the KOs, measured by oil red staining (Fig. S1D). Consistent with the thermogenic effect in adipocytes, *in vivo,* ADAM17 KOs maintained on a standard diet expressed higher levels of thermogenic genes such as *Ucp1*, *Pgc1α*, *Prmd16*, and *Dio2* in their interscapular BAT than their WT counterparts (Fig. 1H). Our data indicate that *Adam17* mRNA and protein levels and sheddase activity are modulated by the neurotransmitter NE to repress thermogenesis. This led us to investigate the hypothesis that ADAM17 could serve as a rheostat, licensed by adrenoceptor stimulation, to limit the overactivation of the thermogenic programs in adipocytes.

3.2. ADAM17 deletion in adipocytes is anti-obesogenic and promotes increased energy expenditure via elevated non-shivering thermogenesis

The observation of elevated expression of thermogenic genes in primary adipocytes and in the interscapular BAT from lean mice, together with the previous observation that ADAM17 KO [38] or iRhom2-

deficient mice [43] have a hypermetabolic phenotype could imply that loss of ADAM17 drives enhanced energy expenditure via non-shivering thermogenesis *in vivo*. To test this, we assessed metabolic parameters such as body weight, food intake, and energy expenditure in our WT and KO mice maintained on a standard diet. As shown in Fig. S2A and B, no significant differences were observed in the body mass and food intake of WT and KO mice. Notably however, the KO mice showed a significant increase in total energy expenditure and oxygen (O_2) consumption and carbon dioxide (CO_2) production during the dark phase (Figs. S2C—E) which are consistent with the reported hypermetabolic phenotype observed in whole-body ADAM17 KO mice [38]. Like O_2 consumption and CO_2 production, respiratory exchange ratio (RER), a measure of the relative utilization of carbohydrates versus fats as a fuel source [79] is elevated only in the dark phase in the KO mice (Fig. S2F). This enhanced energy expenditure in the KO mice is not accounted for by differences in locomotion between WT and KO mice (Fig. S2G). With the observation of elevated energy expenditure in the KO mice especially in the dark phase (Fig. S2C), we predicted that the KO mice should be protected from obesity since these animals should be better able to expend excess calories. To test this, we allowed WT and KO mice to feed *ad libitum* on a high-fat diet (HFD) for 26 weeks (Fig. S3A and B). Notably, the KO mice gained less body weight and accumulated less fat in adipose tissues relative to the WT mice (Figure 2A—B; Figs. S3A—D), despite consuming more calories than their WT counterparts (Fig. 2C). This increase in food intake was previously observed in lean ADAM17 global KO mice [38]. To assess the overall metabolic phenotypes of these mice and to account for the reduced weight gain in the KOs, we placed the obese mice in metabolic cages and quantified energy expenditure, oxygen consumption, CO_2 production, and overall locomotor activity. To control for the differences in body weight between WT and KO mice on HFD in our study of energy expenditure, oxygen consumption and CO_2 production, we analyzed our data using analysis of covariance (ANCOVA), introducing body weight as a covariate [80] As shown in Figure 2D—F, the KO mice expended more energy, consumed more oxygen, and produced more CO_2 relative to the WT mice suggesting that protection of KO mice from obesity is driven by increased metabolic rate. While the respiratory quotient (Fig. 2G) and locomotor activity (Fig. 2H) of KO mice were unremarkable, notably, we observed a significant increase in BAT thermogenesis (Fig. 2I). As the core body temperature of KOs was unaltered compared to WT mice, (Fig. 2J), we conclude that under an obesogenic regime, KO mice are hypermetabolic and expend

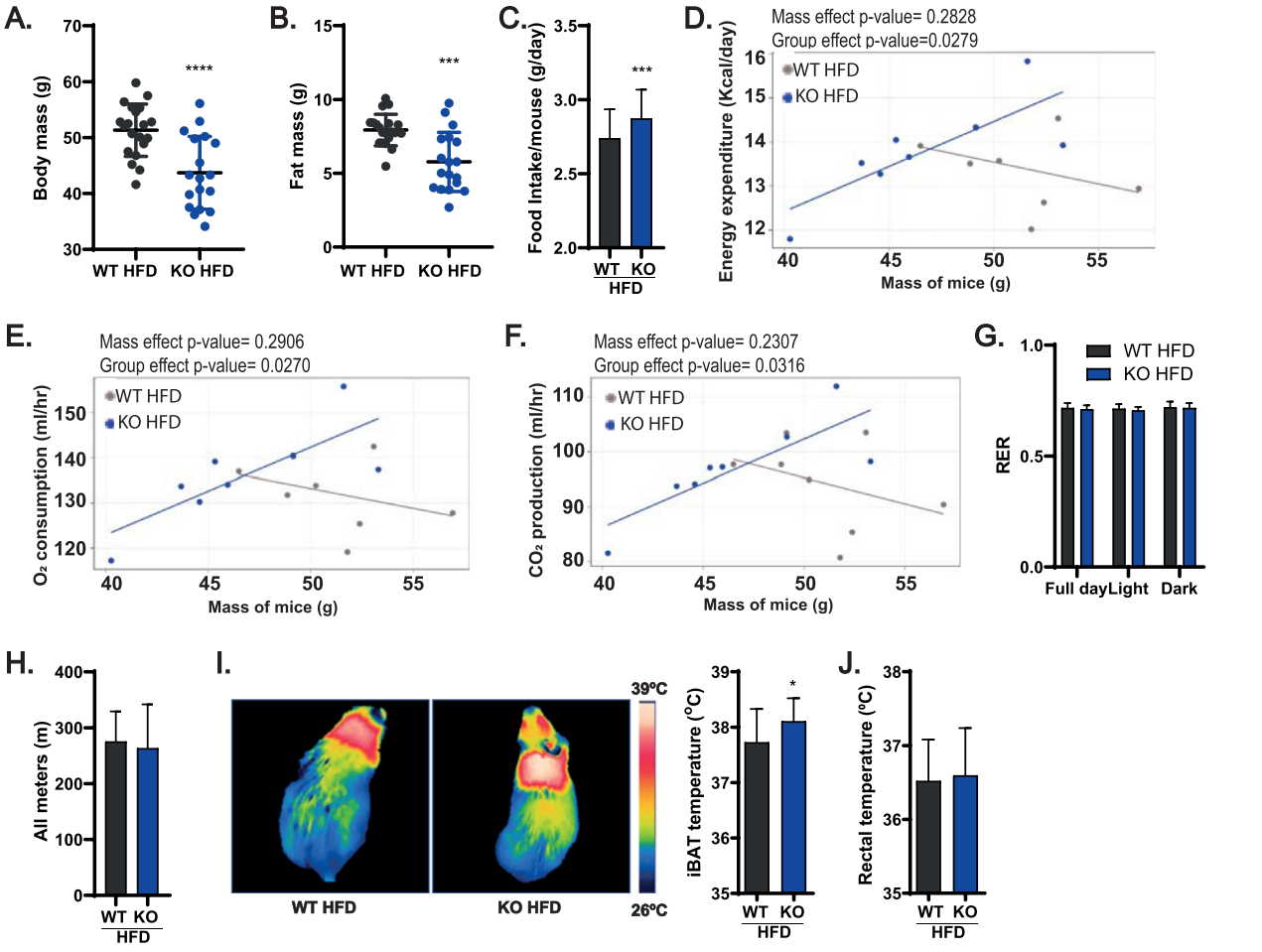

Figure 2: Mice null for ADAM17 in adipocytes are less prone to developing diet induced obesity by increasing energy expenditure. **(A—C)**, Body mass (**A**), pooled fat mass (visceral adipose tissues, inguinal adipose tissue, and iBAT) (**B**), and mean daily food intake per mouse (**C**) of WT and KO mice on high-fat diet (HFD) for 26 weeks (WT n = 20, KO n = 18). **(D—F)**, Scatter plots of energy expenditure (**D**), oxygen consumption (**E**), and carbon dioxide production (**F**) over 24 h in obese WT and KO mice with body mass used as a covariate (WT n = 8, KO n = 7). **(G—H)**, Respiratory exchange ratio (RER) (**G**), and distance covered (**H**) over 24 h period of WT and KO mice on HFD for 26 weeks (WT n = 8, KO n = 7). **(I-J)**, Thermographic representation and quantification of temperature of the interscapular region (**I**), and rectal temperature (**J**) of WT and KO mice after 26 weeks on HFD (WT n = 16, KO n = 17). Results presented as mean ± SD. *P < 0.05, **P < 0.01, ***P < 0.001, ****P < 0.0001.

significantly more energy on thermogenesis than their WT counterparts. These data support the hypothesis that ADAM17 is an endogenous inhibitor of thermogenesis.

3.3. ADAM17 deletion protects from obesity-associated adipocyte hypertrophy in some fat depots by enhancing the expression of genes involved in lipid catabolism and thermogenesis

As KO mice were protected from obesity and exhibited an overall reduction in fat mass, we next sought to establish which adipose depots were most affected. We found that except for the epididymal WAT (where a statistically non-significant trend towards reduced mass in the KO was observed) (Figure 3A) the visceral adipose tissues (mesenteric and retroperitoneal WATs) (Figure 3B,C), the inguinal WAT (Fig. 3D), and the interscapular BAT (Fig. 3E) were significantly reduced in mass in the KOs compared to WT controls. Moreover, for some, but not all, fat depots tested, we found that the KO mice exhibited reduced adipocyte area (Figure 3F—J). Consistent with our previous data showing elevated thermogenic gene expression in ADAM17-deficient BAT (Fig. 1H), upon exposure to HFD, the BAT of KO mice better retained its characteristic multilocular lipid droplet morphology (Fig. 3J) with increased LD number per unit area (Fig. 3K) compared to WT controls. We further analyzed how ADAM17-deficient white adipose tissues (epididymal and inguinal) better adapt to an obesogenic diet than their WT counterparts. Adipose tissue expansion is due to two mechanisms: hyperplasia (an increase in adipocyte numbers within the tissue) versus hypertrophy (an increase in adipocyte cell size) [81]. Notably, the KO WATs expressed significantly higher levels of mRNA of the adipogenic genes *Pparγ* and *C/ebpα* that promote adipose tissue hyperplasia and *de novo* adipocyte recruitment, relative to the WT controls (Fig. 3L-M). Furthermore, as the KOs had reduced adipocyte area per adipose tissue region in some fat depots (Fig. 3G, I-J), this implies that the KOs had increased number of adipocytes. In addition, there was an increase in the mRNA levels of the lipolytic genes *Atgl* and *Hsl* in the WATs from the KO mice (Fig. 3L-M). An increase in adipogenesis (hyperplasia) and elevated lipolysis could account for the decreased adipose tissue mass encountered in the KO mice. The ratio of the lipolysis products released into circulation versus those oxidized and liberated as heat within adipose tissues is critical in determining whether lipids are ectopically deposited in other metabolic organs, such as the liver [82]. Notably, ADAM17-deficient WATs have elevated expression of genes involved in lipid oxidation (Fig. 3L-M) while elevated expression of thermogenic genes was found in the inguinal WAT and interscapular BAT of the KO mice (Fig. 3N-O). Hence, the potentially elevated partitioning of ingested lipids towards catabolism, and BAT thermogenesis and inguinal WAT beiging could spare the KO mice from adiposity and ectopic fat accumulation.

3.4. Loss of ADAM17 protects from obesity-driven hepatic lipid spillover, insulin resistance, and adipose tissue inflammation

Consistent with the notion of better lipid handling implied by the elevated expression of genes associated with lipid oxidation, the KO mice on HFD were significantly protected from obesity-induced liver enlargement (Figure 4A) and lipid accumulation (Figure 4B—C), associated with reduced liver triglyceride accumulation compared to WT controls (Fig. 4D). We did not detect development of fibrosis in the livers of both genotypes by performing Masson's trichrome staining (data not shown), and the liver function was unaltered by measuring the levels of ALT and AST in the serum (Fig. S4A). To further understand whether the protection from hepatosteatosis in KOs results from a reduced propensity for this organ to uptake, store, or export lipids, we quantified the mRNA expression of genes involved in these processes. As shown in Fig. S4B, the expression of the fatty acid transporter *Cd36* was significantly downregulated in the livers of KO mice compared to WT controls, possibly because of their leaner phenotype, as the expression of CD36 is promoted during obesity [83,84]. Furthermore, consistent with the improved metabolic health of the KO animals, genes involved in the positive regulation of lipolysis and lipid oxidation (Figs. S4C—D) were upregulated in the liver of KO mice compared to WT controls. In addition, we found an upregulation of the mRNA levels of transcripts that regulate the formation and export of lipoproteins from the liver, such as *Apob1* and *Apoe,* in KO livers compared to WT controls (Fig. S4E). Together, these results show that loss of ADAM17 in adipose tissues protects from lipotoxicity-derived non-alcoholic fatty liver disease (NAFLD) development typified by increased hepatic lipid uptake, and decreased oxidation and export [83]. Consistent with the notion that the capacity of the liver to handle lipids has an important impact on the serum lipid profile and upon metabolic health in general, we observed significantly lower levels of total cholesterol and LDL-cholesterol in the serum of KO mice compared to WT animals fed on HFD (Figure 4E&G), with no change in serum triglyceride levels (Fig. 4F). Because of lower levels of circulating cholesterol associated with the observed healthier adipose tissues (Fig 3A-M), KO mice exposed to obesogenic conditions presented lower fasting glycaemia and insulinaemia, and were more insulin sensitive (Figure 4H—J). The subjection of these mice to glucose or insulin tolerance tests confirmed that the KO mice on HFD are more glucose tolerant and insulin sensitive, respectively, relative to obese WT mice (Figure 4K&M), indicating that the KO mice were protected from obesity-associated glucose metabolism alterations. This observation is further consolidated by the significantly lower area under the curve (AUC) for the glucose levels of KO mice observed in the glucose and insulin tolerance tests (Figure 4L&N). Notably, no differences were observed in the lipid profile (Figs. S4F—H), fasting glycaemia and insulinaemia (Figs. S4I—J) and insulin and glucose tolerance (Fig. S4K-L) in KO *vs* WT mice maintained on standard diet (SD). Hence, loss of ADAM17 in adipose tissues has the most noticeable impact within the context of positive energy balance associated with an obesogenic diet.

As ADAM17 plays a role in the dissemination of inflammatory responses, we next assessed whether its deletion affected HFD-triggered adipose tissue inflammation. Notably, consistent with our observation that ADAM17-deficient adipose tissues exhibited reduced mass and adipocyte size (Figure 3A—K) and the animals were protected protection from insulin resistance (Fig. 4H-L), histopathological analysis of crown-like structures (which are synonymous within macrophage infiltration [85]) from WATs show that the eWAT from the KOs had fewer inflammatory infiltrates (Fig. S5A). Consistent with this, eWAT from KO mice also expressed lower mRNA levels of inflammatory genes (Fig. S5B). Flow cytometry analysis of the polarity of macrophages within the eWAT showed that macrophages in the eWAT of the KO mice were relatively more M2-polarized compared to those from the WT. These macrophages (from KO eWAT) expressed lower proportions of the M1 marker CD11c and higher proportions of the M2 marker CD206, respectively (Fig. S5C). No differences were observed in the extent of crown-like structures in inguinal WAT of WT versus KO mice by histopathological analysis (Fig. S5D). Expression of IL1β was reduced in the inguinal WAT from the KO mice (Fig. S5E), while flow cytometry analysis showed that macrophages from the inguinal WAT of KO mice express higher level of the M2 marker CD206 (Fig. S5F). The gating strategy for flow-cytometry is shown in Fig. S5G.

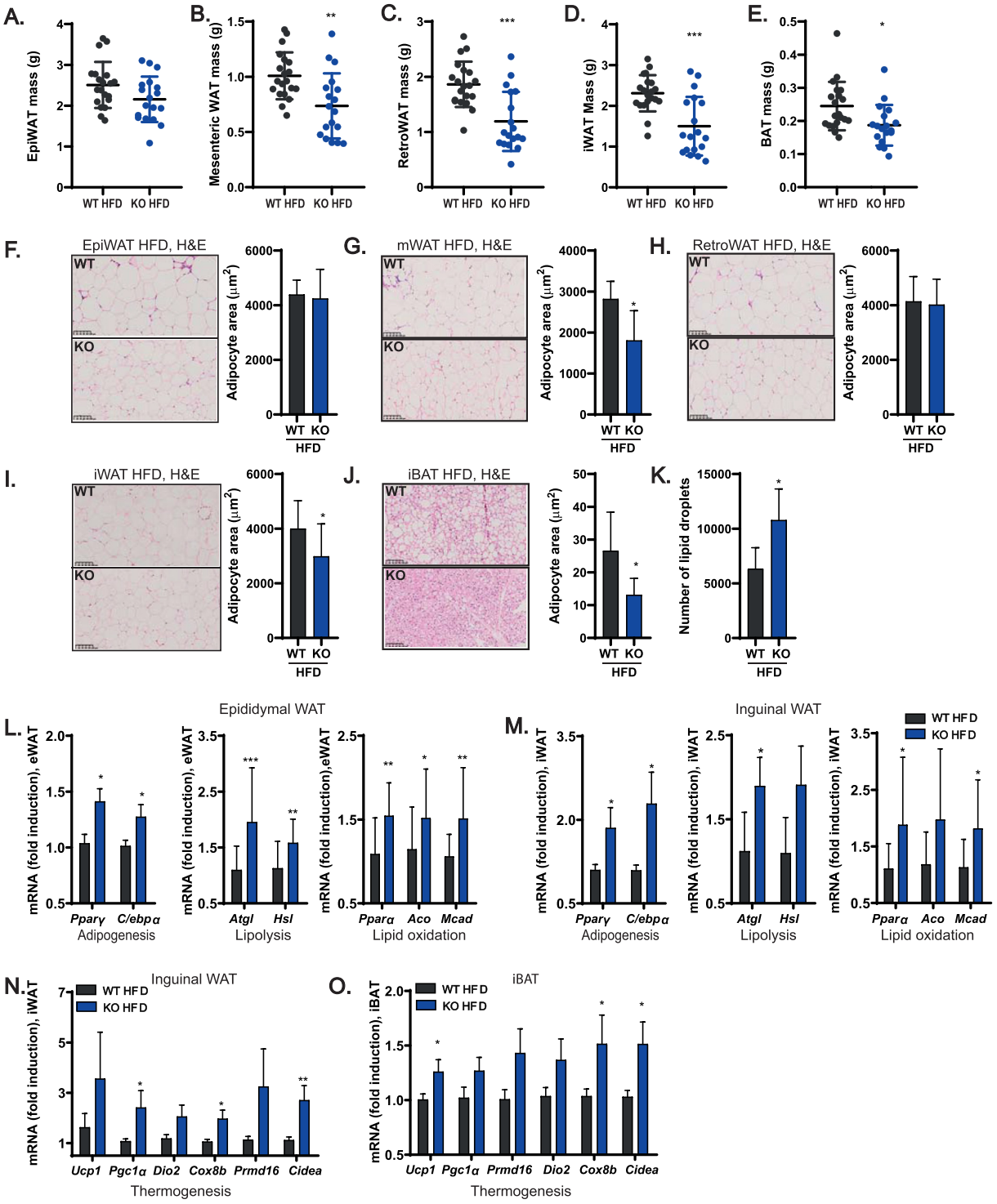

Figure 3: Mice null for ADAM17 in adipocytes are protected from white adipocyte hypertrophy and brown adipocyte whitening on HFD. **(A–E)**, Mass of epididymal (**A**), mesenteric (**B**), retroperitoneal (**C**), inguinal (**D**), and interscapular brown (**E**) adipose tissues of WT and KO mice after 26 weeks of HFD (WT n = 20, KO n = 18). **(F–J)**, H&E staining and quantification of adipocyte size (area) from epididymal (**F**) (WT n = 11, KO n = 13), mesenteric (**G**) (WT n = 6, KO n = 6), retroperitoneal (**H**) (WT n = 7, KO n = 7), inguinal (**I**) (WT n = 12, KO n = 12), and interscapular brown (**J**) (WT n = 6, KO n = 6) adipose tissues of WT and KO mice on HFD. **(K)**, Quantification of lipid droplets from H&E stained iBAT slides of WT and KO on HFD (WT n = 6, KO n = 6). **(L)**, mRNA levels of adipogenic (WT n = 12, KO n = 12), lipolytic (WT n = 20, KO n = 18), and lipid oxidation (WT n = 19, KO n = 17) related genes in the epididymal adipose tissue of WT and KO mice on HFD. **(M)**, mRNA levels of adipogenic (WT n = 18, KO n = 15), lipolytic (WT n = 18, KO n = 15), and lipid oxidation (WT n = 18, KO n = 15) related genes in the inguinal adipose tissue of WT and KO mice on HFD. **(N–O)**, mRNA level of thermogenic genes in the inguinal (**N**) (WT n = 17, KO n = 15) and interscapular brown (**O**) (WT n = 18, KO n = 14) adipose tissue of WT and KO mice on HFD. Results presented as mean ± SD. *P < 0.05, **P < 0.01, ***P < 0.001, ****P < 0.0001. (For interpretation of the references to color in this figure legend, the reader is referred to the Web version of this article.)

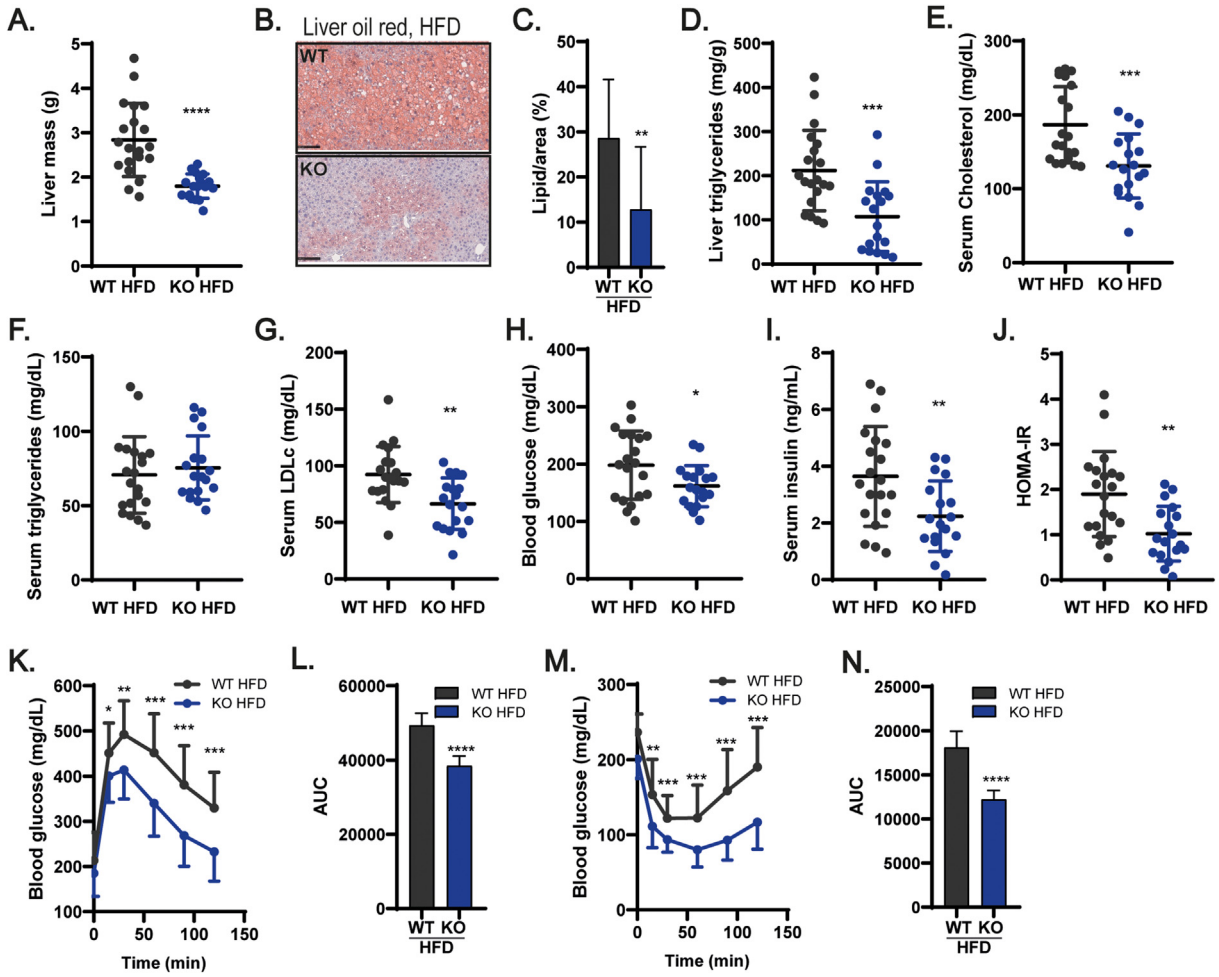

Figure 4: Mice null for ADAM17 in adipocytes are protected against HFD induced ectopic lipid deposition in the liver, dyslipidemia, and systemic insulin resistance. **(A–C)**, Mass of liver (**A**) (WT n = 20, KO n = 18) and images of oil-red stained liver samples (**B**) (WT n = 13, KO n = 13), and quantification of percentage of lipid-laden area of oil-red stained liver samples (**C**) (WT n = 13, KO n = 13), from WT and KO mice after 26 weeks of HFD. **(D)**, Triglyceride content of liver from WT and KO mice on HFD (WT n = 20, KO n = 18). **(E–G)**, Fasting serum levels of total cholesterol (**E**), triglycerides (**F**), and low-density lipoprotein-cholesterol (LDLc) (**G**) in WT and KO mice on HFD (WT n = 20, KO n = 18). **(H–I)**, Fasting blood glucose (**H**) and serum insulin levels (**I**) in WT and KO mice on HFD (WT n = 20, KO n = 18). **(J)**, Homeostatic assessment model for insulin resistance (HOMA-IR) in WT and KO mice on HFD (WT n = 20, KO n = 18). **(K-L)**, Glucose tolerance test (GTT) (**K**) and the area under curve (AUC) of glucose levels during GTT (L) in WT and KO mice on HFD (WT n = 20, KO n = 18). **(M–N)** Insulin tolerance test (ITT) (**M**) and the area under curve (AUC) of glucose levels during ITT (**N**) in WT and KO mice on HFD (WT n = 20, KO n = 18). Results presented as mean ± SD. *P < 0.05, **P < 0.01, ***P < 0.001, ****P < 0.0001. (For interpretation of the references to color in this figure legend, the reader is referred to the Web version of this article.)

3.5. Semaphorin 4B is a novel ADAM17 substrate expressed in adipocytes and regulated by thermogenic stimuli and obesity

Our results so far show that ADAM17 ablation in adipocytes protects from the metabolic alterations associated with an obesogenic diet by promoting energy expenditure in adipose tissues. This predicts that proteolytic shedding of substrate(s) by ADAM17 from the cell surface of adipocytes should drive signaling pathways that negatively regulate energy expenditure. As stated earlier, the major pathways regulated by ADAM17 are the TNFR and the EGFR signaling pathways. However, neither of these pathways has been compellingly shown to contribute to adipose tissue thermogenesis or weight gain upon exposure to HFD [40–42,86,87] and their reported roles in metabolic diseases are often contrasting [88]. Another critical pathway mediated by ADAM17 proteolysis, IL-6 *trans*-signaling, exerts its salutary metabolic effects centrally by reducing food intake and by promoting energy expenditure [89]. The action of IL-6 hence promotes weight loss and decreases body fat [89–92]. Although our adipose tissue-specific ADAM17 mutants exhibited elevated food intake, which could be interpreted as an impact of loss of IL-6-*trans* signaling (Fig. 2C) they are nonetheless hypermetabolic and less susceptible to weight gain on HFD (i.e., the opposite phenotype observed upon blockade of IL-6-*trans* signaling in the brain [88]). Hence although we have not experimentally ruled this out in our model and accept that ADAM17 exerts complex and pleiotropic effects in multiple organ systems via the shedding of multiple key substrates, this implies that defective IL-6 *trans*-signaling does not underpin the basis of the anti-obesogenic and hypermetabolic phenotype observed in our model. We therefore adopted an objective proteomic approach to interrogate the secretome from WT versus ADAM17 KO primary inguinal and brown adipocytes to identify ADAM17 substrates secreted in thermogenic adipocytes. We used hiSPECs (high-performance secretome protein enrichment with click sugars), an approach that enables the specific labelling and enrichment of glycoproteins by culturing cells with an azido group-containing sugar [93]. This approach carries the advantage that cells can be grown under normal serum-containing conditions [93]. As shown in the schematic, Figure 5A, out of the total proteins detected in the WT

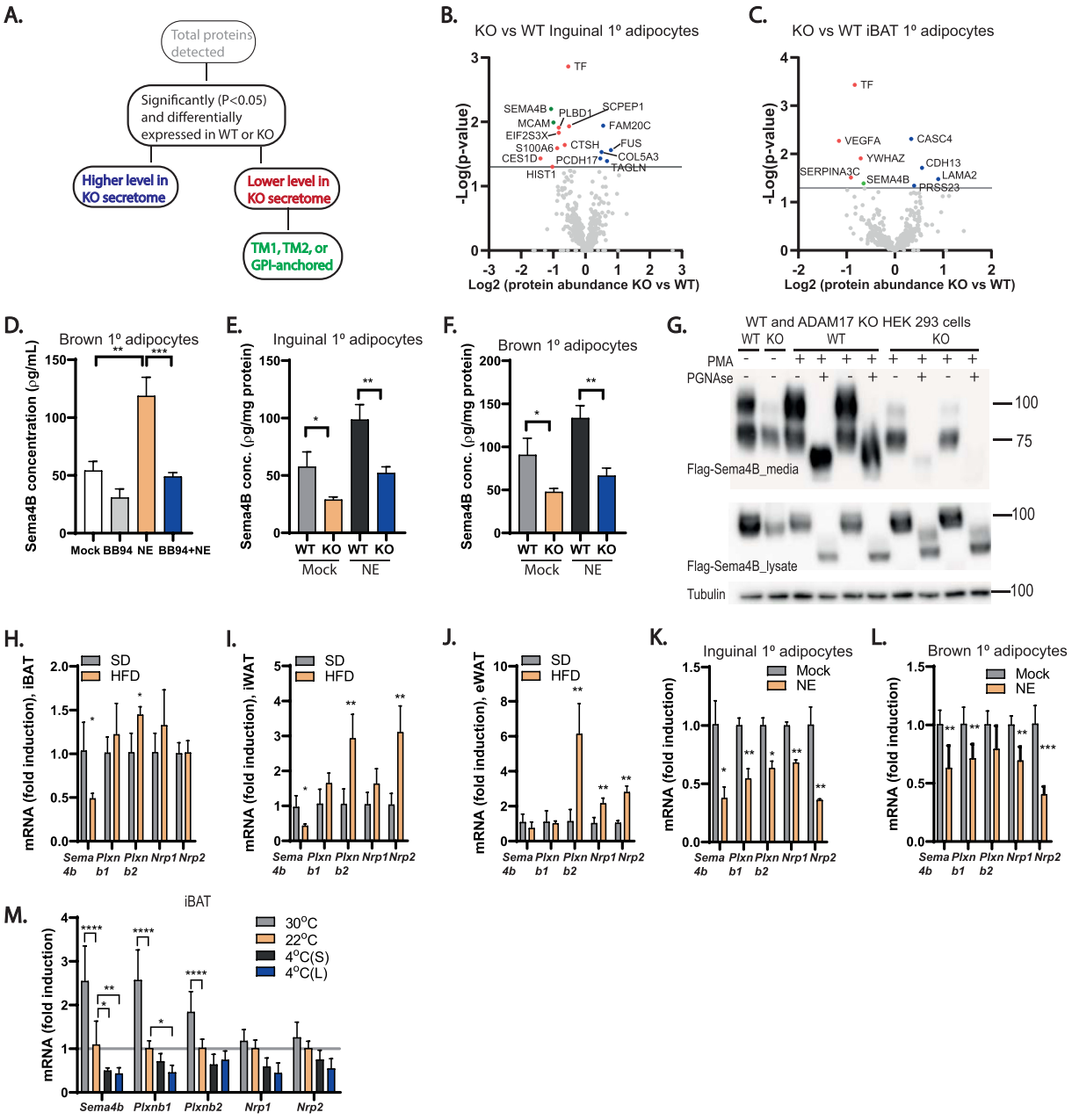

Figure 5: Semaphorin 4B is a novel adipokine and an ADAM17 substrate. **(A)**, Schematic showing how the potential ADAM17 substrates were arrived at. Proteins denoted by grey circles detected by the mass spec at a P value of >0.05 were excluded, as were proteins whose levels were elevated in ADAM17 KO secretomes (denoted in blue circles). Proteins whose levels were downregulated in ADAM17 KO secretomes are denoted in red circles while the small subset of these that fulfill the characteristics of known ADAM17 substrates (TM1, TM2 or GPI-anchored [63]) are denoted by green circles. **(B–C)**, Volcano plot depicting proteins detected in the secretome of ADAM17 KO vs WT inguinal (**B**) or brown (**C**) primary adipocytes. Proteins with log2 difference greater than or less than zero are detected at higher or lower levels, respectively in conditioned medium from ADAM17 KO adipocytes. Proteins above the horizontal cut-off (-Log pvalue = 1.3) are significantly detected at higher or lower levels in conditioned medium from ADAM17 KO adipocytes (n = 5). **(D–F)**, Sema4B levels quantified by ELISA in conditioned media from WT brown primary adipocytes treated with or without 10 μM of the metalloprotease inhibitor, batimastat (BB-94) and 2 μM norepinephrine (NE) **(D),** WT and ADAM17 KO primary inguinal (**E**) and brown (**F**) adipocytes with or without stimulation with 2 μM of NE for 10 h (n = 3). **(G),** Immunoblot of Sema4B in conditioned media from WT and ADAM17 KO Hek293 cells transfected with full-length Sema4B plasmid. Cells were either untreated or treated with 1 μM phorbol myristate acetate (PMA) and deglycosylated using PNGAse. Immunoblots for tubulin serve as a loading control. (n = 4). **(H–J)**, mRNA levels of *Sema4b* and its receptors; *Plxnb*1 & 2, *Nrp*1 & 2 in the interscapular BAT (**H**), inguinal WAT (**I**), and epididymal WAT (**J**) of lean and HFD-induced obese mice (n = 4). **(K–M),** mRNA levels of *Sema4b* and its receptors *Plxnb1 & 2, Nrp1 & 2* in inguinal **(K)** and brown **(L)** primary adipocytes treated without or with 2 μM NE (n = 5), and in the interscapular BAT **(M)** of mice exposed to different ambient temperatures; thermoneutrality (30 °C) (10 days), room temperature (22 °C), acute cold exposure (4° S) (4 °C for 6 h), and chronic cold exposure (4° L) (4 °C for 10 days) (n = 6). Results presented as mean ± SD. *P < 0.05, **P < 0.01, ***P < 0.001, ****P < 0.0001. (For interpretation of the references to color in this figure legend, the reader is referred to the Web version of this article.)

and KO adipocyte secretomes, we focused on the proteins that were significantly ($P < 0.05$) and differentially expressed. To identify potential substrate(s) of ADAM17 we further filtered for proteins that were detected at significantly lower levels in the secretome of the KO adipocytes (i.e., proteins that are potential ADAM17 substrates whose shedding into the secretome are reduced because of loss of ADAM17). Of these proteins, based on known features of ADAM17 substrates, only proteins containing a single transmembrane domain (TM1),TM2, or GPI-anchored proteins were considered to be potential ADAM17 substrates [63]. Taking these factors into account, we observed a significant reduction in the levels of the cleaved forms of the transmembrane proteins Semaphorin 4B (Sema4B) and melanoma cell adhesion molecule (MCAM) in the secretome from the KO inguinal adipocytes, while only observing a reduction in the level of Sema4B in the secretome from the KO brown primary adipocytes (Figure 5B–C). As Sema4B was hence significantly reduced in the secretome from both the brown and inguinal adipocytes (as also shown in Tables 4 and 5) and we decided to investigate its role in adipocyte physiology further. Semaphorins are secreted, transmembrane and cell-surface-attached proteins that signal mainly by interaction with Plexin receptors, and act on axonal guidance, and regulate morphology and motility of many cell types [94]. We confirmed that Sema4B is a genuine novel ADAM17 substrate which can be released in response to NE stimulation by quantifying the levels of Sema4B by ELISA in media obtained from unstimulated and NE-stimulated adipocytes. As shown in Figure 5D, the metalloprotease inhibitor BB94 blocked the NE-induced shedding of endogenous Sema4B in immortalized WT adipocytes. When we assessed Adam17 KO primary inguinal (Fig. 5E) and brown (Fig. 5F) adipocytes we found that under unstimulated conditions, the media from KO adipocytes contained significantly lower levels of Sema4B as did NE-stimulated cells. To show that Sema4B shedding activity of ADAM17 is not restricted to adipocytes, we stimulated ADAM17 activity in WT and Adam17 KO HEK293 cells overexpressing full-length form of Sema4B (flag-tagged) using PMA. We compared the expression of Sema4B in the supernatants from these cells with or without PMA treatment (Fig. 5G). Interestingly, these data confirmed that ADAM17 can shed Sema4B in other tissues. Moreover, as we detected a lower molecular weight form of Sema4B whose shedding was unabated in ADAM17 KO cells, this may suggest that additional proteases may potentially contribute to Sema4B shedding in some contexts. To understand if Sema4B may play a role in obesity and adipose tissue thermogenesis, we evaluated mRNA expression of Sema4B and its receptors (plexins and neuropilins) in adipose tissues from obese mice and lean mice exposed to different ambient temperatures. In obese mice, the expression of *Sema4B* was also downregulated in interscapular BAT and inguinal WAT but not in epididymal WAT (Figure 5H–J). However, the expression of its receptors and coreceptors was upregulated in these fat depots in obese animals (Figure 5H–J). A key feature of genes involved in thermal regulation (e.g. *Ucp1*) is the modulation of their transcriptional levels by thermogenic cues in response to sympathetic outflow and consequent β-adrenoceptor activation [95]. Intriguingly, we found that the mRNA levels of *Sema4b* and its known receptors (Plexins) and co-receptors (Neuropilins [96]) were significantly downregulated in response to NE stimulation of primary inguinal and brown mouse adipocytes (Figure 5K,L). Furthermore, the levels of *Sema4b* and its associated receptors/co-receptors correlated with exposure of mice to ambient temperature, decreasing in expression levels from thermoneutrality to 4 °C (Fig. 5M), which is potentially consistent with a negative role in thermogenesis regulation. Taken together, these data indicate that *Sema4b* expression levels are significantly affected by ambient temperature, diet-induced thermogenesis, or NE, suggesting that SEMA4B is implicated in the regulation of thermogenesis.

3.6. Expression of SEMA4B/ADAM17 pathway genes is regulated in human obese adipose tissues and upon weight loss intervention

To investigate if this novel pathway mediated by Sema4B cleavage by ADAM17 in adipocytes could have an impact in human obesity, we measured the mRNA levels of *SEMA4B, PLEXIN (PLXN)B1* and *2, NEUROPILIN (NRP) 1* and *2, ADAM17*, and of its known critical regulator *iRHOM2* in human adipose tissues. The anthropometric and biochemical parameters of participants in our cross-sectional study are shown in Table 2. There we verified that in obese (BMI>30 kg/m2) compared to non-obese subjects *PLXNB2, NRP2* and *iRHOM2* mRNA level was increased in the omental WAT (VAT), while in abdominal subcutaneous WAT (SAT) the mRNA expression of *NRP2, ADAM17 and iRHOM2* was upregulated (Fig. 6A). Accordingly, a positive correlation between BMI and the mRNA level of *PLXNB2, NRP2, and iRHOM2* in VAT, and with *IRHOM2* and *ADAM17* gene expression in SAT was observed (Table 3). Interestingly, after weight loss by bariatric surgery, a heat map of microarray data from SC adipose tissues from 16 obese women at the baseline and follow up [75] shows a reduction in the expression of *IRHOM2, ADAM17, PLXNB2*, and *NRP2* (Fig. 6B). RT-PCR assays performed on SC adipose tissue from an extended sample of 23 female obese patients at the baseline and after bariatric surgery (Table 4) shows that the mRNA levels of *PLXNB1, PLXNB2, NRP1* and *NRP2, ADAM17*, and *iRHOM2* are significantly decreased after weight loss, while the level of *SEMA4B* remains unchanged (Fig. 6C). To understand whether the duration of post-bariatric surgery has an effect on the regulation of these genes, RMA (robust multichip average) were retrieved from the study by Kerr et al. [97]. There, biopsies of SC adipose tissues were obtained from non-obese subjects and obese subjects undergoing bariatric surgery. In the later, fat samples were assessed at the baseline, and 2 and 5 years post-surgery [97]. As shown in Figure 6D, many of the changes in gene expression values shown 2 years post-intervention remained the same 5 years after intervention. Furthermore, the analysis of datasets on human stem cells differentiated into mature brown adipocytes [60] showed that the expression of Sema4B is regulated during adipogenesis (Fig. S6A), and that the treatment of adipocytes differentiated from human subclavicular BAT or SAT with NE [61] downregulates the gene expression of *SEMA4B* (Fig. S6B), as we observed in primary mouse adipocytes (Figure 5J,K). Moreover, gene set enrichment analysis (GSEA) from the datasets from Din et al. [98] showed that enhanced BAT thermogenesis (e.g. increased *Ucp1* expression) in response to ingestion of mixed carbohydrate diet negatively correlates with genes involved in semaphorin and plexin signaling (Fig. S6C). Taken together, these data indicate that SEMA4B may be involved in human adipocyte differentiation and thermogenic function, and that SEMA4B/ADAM17 pathway may contribute development of obesity. Further studies are required to understand the role of this pathway in obesity and adipose tissue thermogenesis and browning.

3.7. Sema4B is a negative regulator of adipogenesis and thermogenesis

As ADAM17 cleaves Sema4B and thermogenic cues in multiple contexts can modulate *Sema4B* mRNA levels, we next tested the effects of cleaved Sema4B upon thermogenic, lipolytic and adipogenic gene expression in a range of models. Strikingly, we observed that stable expression of a truncated/cleaved and hence soluble mimetic of Sema4B (hence tSema4B) in immortalized WT brown adipocytes significantly inhibited *Ucp1* expression in naïve and NE-stimulated

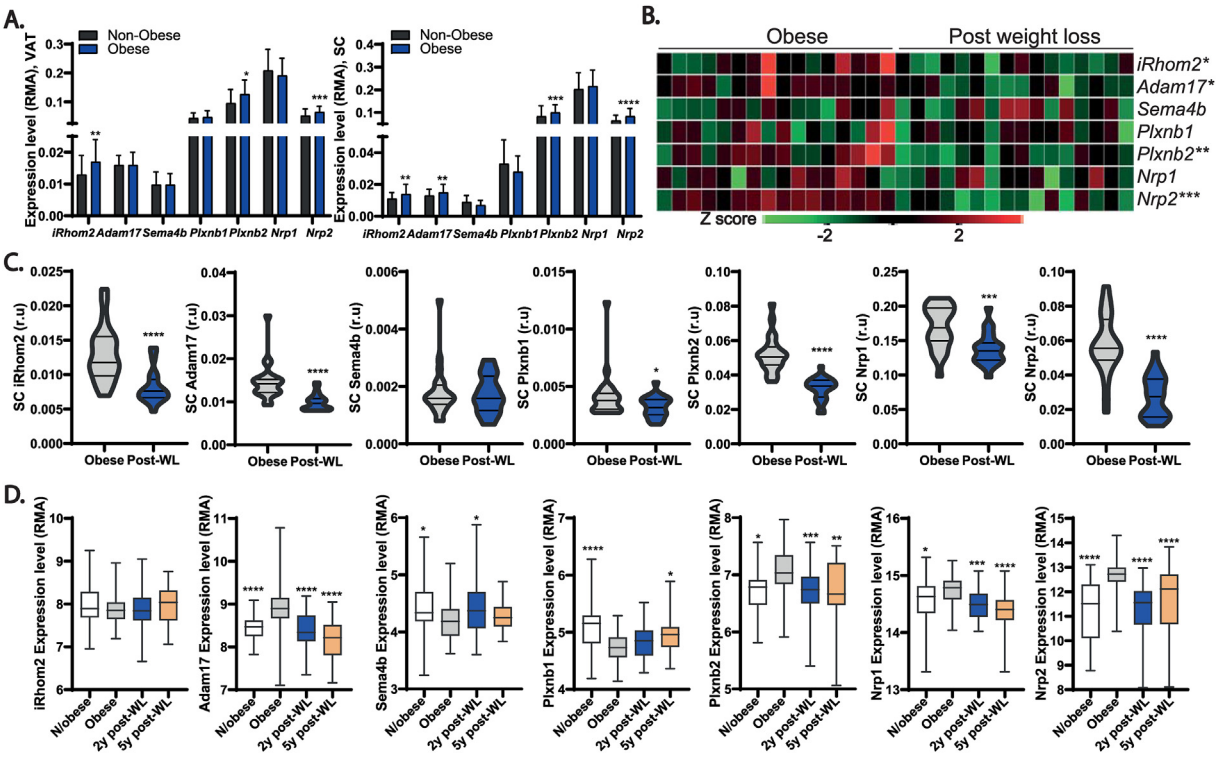

Figure 6: The SEMAPHORIN 4B/ADAM17 pathway is modulated in human obesity and after weight loss intervention. **(A),** mRNA level of *SEMA4B, PLEXIN (PLXN)B1 and 2, NEUROPILIN (NRP) 1 and 2, ADAM17 and of iRHOM2* in omental WAT (VAT) and in abdominal subcutaneous WAT (SAT) from human patients in obese versus lean subjects (non-obese n = 76, obese, BMI $\geq$30 kg/m^2 n = 105). **(B),** Heat map from microarray measurements of the genes, *SEMA4B, PLEXIN (PLXN)B1 and 2, NEUROPILIN (NRP) 1 and 2, ADAM17 and of iRHOM2* of subcutaneous adipose tissue from 16 obese female subjects at baseline and after bariatric surgery. The heat map indicates Row Z-score [-5 to 5] (green-red), calculated by subtracting the overall average microarray signal intensity from raw results in each transcript, and dividing that result by the standard deviation (SD) of measured values across all samples. **(C),** RT-PCR quantification of the levels of the genes *SEMA4B, PLEXIN (PLXN)B1 and 2, NEUROPILIN (NRP) 1 and 2, ADAM17 and of iRHOM2* of subcutaneous adipose tissue from 23 obese female subjects at baseline and after bariatric surgery. **(D),** Robust multichip average (RMA) expression measurements retrieved from the study of Kerr et al. [97] showing the expression of *SEMA4B, PLEXIN (PLXN)B1 and 2, NEUROPILIN (NRP) 1 and 2, ADAM17 and of iRHOM2* in biopsies from the subcutaneous abdominal adipose tissue of 50 obese subjects at the baseline and 2 (49 subjects) and 5 (38 subjects) years post-bariatric surgery, and also from a non-operated group of 28 healthy weight women matched for age. The Student t-test was used. Results presented as mean $\pm$ SD. *P $<$ 0.05, **P $<$ 0.01, ***P $<$ 0.001, ****P $<$ 0.0001. (For interpretation of the references to color in this figure legend, the reader is referred to the Web version of this article.)

mouse adipocytes (Figure 7A). Brown adipocyte differentiation is important for determining the thermogenic capacity of adipocytes while lipolysis is essential for Ucp1 activation. Therefore, these two key processes may be impacted by Sema4B to repress thermogenesis. Indeed, tSema4B repressed the expression of the major lipolytic genes, *Atgl/Pnpla2* and *Hsl* (Fig. 7B) while repressing expression of the adipogenic genes, *Pparγ* and *C/ebpα* (Fig. 7C). Furthermore, in independent experiments, mammalian-produced recombinant tSema4B similarly repressed *Ucp1* levels in primary brown adipocytes in response to NE (Fig. 6D) and downregulated the expression of lipolytic genes (Fig. 7E). A reduction in *C/ebpα* gene expression was also observed, although the difference was not statistically significant (Fig. 7F). Hence, our data suggest that ADAM17, through Sema4B cleavage, secretion and autocrine action on adipocytes, downregulates key processes required to support thermogenesis, including adipogenesis and lipolysis.

To better understand the impact of tSema4B on adipocyte biology in general and specifically to elucidate how tSema4B perturbed processes required to support thermogenesis, we performed RNAseq on WT immortalized primary adipocytes overexpressing tSema4B or the empty vector, under unstimulated (Fig. 7G) versus NE-stimulated conditions (Fig. 7H). Under unstimulated conditions, when a threshold of a log2 fold change of at least 1 or -1 was applied, 543 and 732 genes were upregulated and downregulated (Fig. 7G). Notably, the cohort of genes that were upregulated by tSema4B included Nrp1 (a semaphorin co-receptor that has been reported to bind to Sema4B) plus genes associated with remodeling of the extracellular matrix (Col1a; Fbln1, Fbln2, Timp1). The latter genes, which are expressed at higher levels in fibroblastoid cells such as preadipocytes could indicate that tSema4B impairs adipogenesis. By contrast, prominently downregulated hits were genes involved in lipid metabolism and fatty acid update such Lpl (lipoprotein lipase) the fatty acid transporter CD36 and the fatty acid binding protein Fabp4 and lipolysis (*Atgl/Pnpla2*). As anticipated from the qPCR studies, we also observed downregulation of genes associated with BAT thermogenesis (*Pparγ, Ucp1*). The latter downregulated genes could suggest that Sema4B impairs adipogenesis, curtailing the expression of lipolytic and thermogenic genes. In NE-treated cells, tSema4B expression upregulated and downregulated 540 and 643 genes, respectively (with a log2 fold change of at least 1 or -1) (Fig. 7H). Similar to unstimulated samples, tSema4B-overexpressing NE-treated cells upregulated hits included mRNAs involved in extracellular matrix remodeling (*Col18a1, Serpinf1, Adamts1,Vcam1*) whose expression is higher in fibroblastoid cells and vasculogenesis (*Fbn1* and *Nrp1*). As for mock-treated cells,

Table 4 — Anthropometric and biochemical data of morbid obese women before (baseline) and after (post-weight loss) bariatric surgery and the subsequent weight loss/metabolic improvement (n = 23 women).

Parameters	Baseline	Post-weight loss	p-value[a]
Age (yrs)	48 ± 10	51 ± 10	**<0.0001**
BMI (kg/m^2)	43.4 ± 5.0	29.2 ± 5.7	**<0.0001**
Fat mass (%)	56.2 ± 7.5	39.9 ± 7.7	**<0.0001**
SBP (mmg)	129.2 ± 13.8	129.0 ± 16.3	0.946
DBP (mmg)	79.3 ± 10.2	74.0 ± 12.8	0.111
Glucose (mg/dl)	101.2 ± 36.8	87.4 ± 14.1	0.103
HbA1c (%)	5.8 ± 1.4	4.8 ± 1.8	0.169
Cholesterol (mg/dl)	179.4 ± 31.7	182.9 ± 53.5	0.716
LDL (mg/dl)	74.1 ± 22.9	55.7 ± 13.5	**<0.0001**
HDL (mg/dl)	99.0 ± 29.8	102.3 ± 27.4	0.544
Triglycerides (mg/dl)	107.9 ± 39.7	81.1 ± 29.8	**0.008**

Values represent the mean ± standard deviation. **S/DBP**: systolic/diastolic blood pressure; **Hb1Ac**: glycated haemoglobin; **H/LDL**: high/low density lipids; [a]Student t-test for non-obese subjects vs. obese participants. **Bold** indicates significant results (p-value <0.05).

downregulated hits included genes associated with fatty acid uptake (*Fabp4, Cd36, Lpl*), lipolysis *(Pnpla2/Atgl)* and BAT thermogenesis (*Ucp1, Adrb3*) (Fig. 7H). When gene enrichment analysis was applied on all differentially expressed genes that passed the $p \leq 0.05$ threshold, amongst the genes repressed by Sema4B under unstimulated conditions, the biological processes represented included brown adipocyte differentiation; fatty acid import, storage and beta oxidation (Fig. 7I). When NE-stimulated, the downregulated hits additionally included genes associated with mitochondrial respiration, while the upregulated hits were enriched in mRNAs associated with extracellular matrix organization, development, and angiogenesis. In summary, our transcriptomic data emphasize that cleaved Sema4B represses several key processes that are required to support thermogenesis, lipolysis and most notably adipogenesis.

As overexpression of tSema4B in adipocytes downregulated the expression of genes involved in adipogenesis, lipolysis and thermogenesis (Figure 7A–C, 7G-H), we decided to confirm whether these pathways were altered in immortalized adipocytes expressing tSema4B. We verified that adipogenesis was impaired in these cells, since oil red staining revealed reduced lipid droplet content of tSema4B-treated cells (Fig. 7J). As shown in Figure 7K, lipolysis was also negatively affected as cells overexpressing tSema4B were minimally responsive to stimulation by NE and produced significantly reduced levels of glycerol (a product of triglyceride catabolism) both constitutively and in response to NE stimulation. Consistent with this, we observed reduced protein levels of the key lipolytic regulators phospho-HSL and ATGL (Fig. 7L). Taken together, our data indicate that tSema4B impacts critically on adipogenesis and lipolysis, processes that are required to support thermogenesis.

4. DISCUSSION

One of the most interesting findings to emerge from the present study is the connection between β-adrenoceptors, a cornerstone of adipocyte physiology, and ADAM17. NE treatment of primary adipocytes stimulates shedding of ADAM17 substrates, modulates ADAM17 expression, while exposure of mice to decreasing ambient temperature (which triggers NE release) upregulates ADAM17 levels. Notably, the effects on ADAM17 behavior observed in our model are similar to the response to the ADAM17 stimulant, PMA, where an initial increase in ADAM17 activity and maturation is followed by a subsequent decrease in expression due to its degradation [99]. Our data identify a negative regulatory loop (summarized in Supplementary Fig. 6E) whereby, in tandem to the canonical induction of thermogenesis and lipolysis, NE also triggers an autocrine negative feedback loop that dampens adipogenesis, lipolysis to impinge negatively upon thermogenesis. This is driven by β-adrenoceptor-mediated stimulation of ADAM17 to shed Sema4B, a novel adipokine. Soluble Sema4B triggers a transcriptional response in preadipocytes that represses the expression of several genes that control processes that are required to support thermogenesis (e.g. adipogenesis, lipid uptake, lipolysis) and *Ucp1* expression itself. Speculatively, when triggered by β-adrenoceptor activation, this novel mechanism, which has similarities to EGFR transactivation [100], may fine-tune adipose tissue responses to thermogenic or

Table 5 — Proteins detected at significantly ($P < 0.05$) lower levels in the secretome from ADAM17 KO primary inguinal adipocytes.

-Log (p value)	P value	Log2 difference	Fold change	Protein symbol	GPI	TM1	TM2
2.86	0.0014	−0.53	0.69	TF	0	0	0
2.20	0.0063	−1.07	0.48	SEMA4B	0	1	0
1.99	0.0103	−0.99	0.50	MCAM	0	1	0
1.93	0.0118	−0.51	0.70	SCPEP1	0	0	0
1.64	0.0230	−0.64	0.64	CTSH	0	0	0
1.43	0.0373	−1.40	0.38	CES1D	0	0	0
1.30	0.0496	−1.03	0.49	HIST1H2BC	0	0	0
1.91	0.0124	−0.83	0.56	PLBD1	0	0	0
1.83	0.0148	−0.83	0.56	EIF2s	0	0	0
1.59	0.0259	−0.88	0.54	S100A6	0	0	0

Table 6 — Proteins detected at significantly ($P < 0.05$) lower levels in the secretome from ADAM17 KO primary brown adipocytes.

-Log (p value)	P value	Log2 difference	Fold change	Protein symbol	GPI	TM1	TM2
3.43	0.0004	−0.83	0.56	TF	0	0	0
2.27	0.0054	−1.16	0.45	VEGFA	0	0	0
1.91	0.0124	−0.71	0.61	YWHAZ	0	0	0
1.51	0.0311	−0.91	0.53	SERPINA3C	0	0	0
1.39	0.0403	−0.65	0.64	SEMA4B	0	1	0

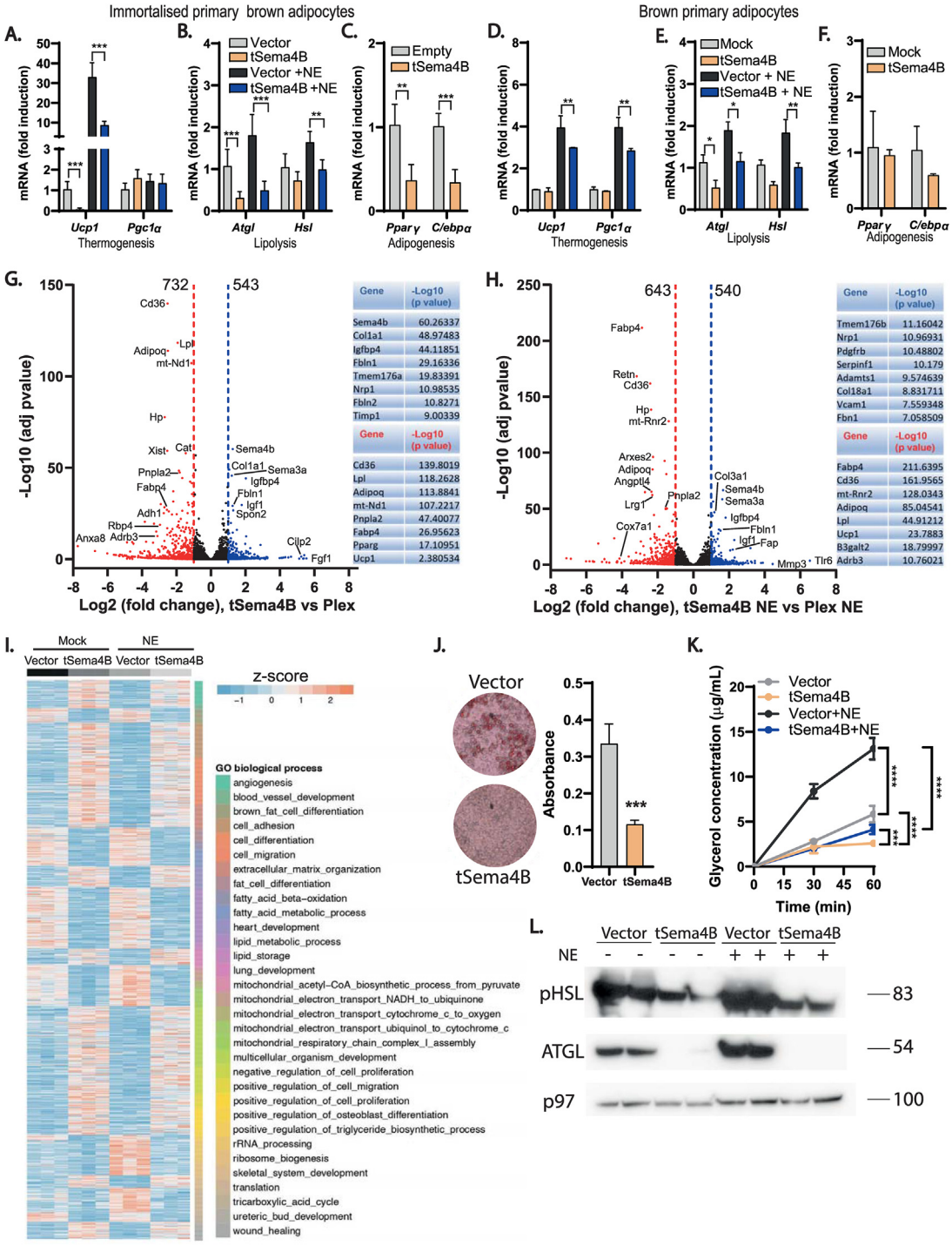

Figure 7: Semaphorin 4B negatively regulates adipogenesis and thermogenesis. **(A–C)**, mRNA expression of the thermogenic **(A)**, lipolytic **(B)**, and adipogenic **(C)** genes in immortalized primary adipocytes transduced with empty vector or truncated Sema4B (tSema4B) and treated with or without NE. (n = 6). **(D–F)**, mRNA expression of the thermogenic **(D)**, lipolytic **(E)**, and adipogenic **(F)** genes in primary adipocytes treated with or without recombinant tSema4B and subsequently treated with or without NE (n = 5). **(G)**, Volcano plots showing differentially expressed genes in immortalized primary brown adipocytes transduced with tSema4B or empty vector (Plex) and a list of some upregulated and downregulated genes by tSema4B (n = 3). **(H),** Volcano plots showing differentially expressed genes in immortalized primary brown adipocytes transduced with tSema4B or empty vector (Plex) in response to NE and a list of some upregulated and downregulated genes by tSema4B in response to NE (n = 3). **(I),** Heat map of upregulated and downregulated genes by tSema4B in naïve and NE-stimulated cells according to the GO:term biological process. **(J),** Oil red staining and quantification of oil red absorbance in differentiated immortalized primary brown adipocytes transduced with empty vector or truncated Sema4B (tSema4B). **(K),** Glycerol levels (pg/mL) in the medium of the cells indicated above under NE exposure or unstimulated conditions **(L),** Immunoblots of the phosphorylated (active) form of the lipolytic enzyme, hormone sensitive lipase (HSL) and the central lipolytic enzyme adipose triglyceride lipase (ATGL) in immortalized primary adipocytes transduced with empty vector or truncated Sema4B (tSema4B) with or without stimulation with NE. A p97 immunoblot is included as loading control. Results presented as mean ± SD. *P < 0.05, **P < 0.01, ***P < 0.001, ****P < 0.0001. (For interpretation of the references to color in this figure legend, the reader is referred to the Web version of this article.)

differentiation cues or act as a negative feedback loop to prevent untrammelled resource depletion to avoid a sustained state of negative energy balance. Our data also reveal that the regulation of the ADAM17-Sema4B axis and candidate Sema4B receptors and co-receptors is highly dynamic. At the post-translational level, NE can induce early ADAM17 activation and Sema4B shedding (e.g. within the timeframe of 1 h, Fig. 1A). Over later timepoints (e.g. 6 h), a complex second tier of events occurs that tunes the levels of mRNAs of ADAM17, Sema4B and its receptors/co-receptors. Moreover, the mRNA levels of these genes respond, in mice, to high fat diet, NE, and ambient temperature while varying according to adipose tissue depot subtype (e.g. brown versus subcutaneous versus; Fig. 5). Our human data are similarly complex, showing that the levels of candidate Sema4B receptors/co-receptors but not necessarily Sema4B itself are elevated during obesity and downregulated in obese subjects following weight loss. Future studies will be required to dissect out how these early and later regulatory aspects impinge on the control of adipogenesis, lipid catabolism and thermogenesis within the context of brown versus subcutaneous adipocytes that are capable of beiging. Future studies will be required to determine whether the Sema4B pathway is actionable for the improvement of metabolic health, for instance to enhance adipocyte recruitment to mitigate the detrimental metabolic effects associated with obesity or to enhance thermogenesis. Our study reveals that ablation of ADAM17 in adipocytes promotes the expression of thermogenic genes (and elevates thermogenesis) in the iBAT of animals on HFD and on SD under standard housing conditions, leading to improved metabolic health of animals on an obesogenic diet. This is reminiscent of the hypermetabolic phenotype reported for the fraction of whole-body ADAM17 KOs that escape perinatal lethality [38]. Our adipose tissue-specific ADAM17-deficient mice also had a marginal increase in energy expenditure on SD, although this appears not to confer easily observable metabolic benefits (e.g. upon glucose homeostasis and lipid profile) relative to WT mice under the sub-thermoneutral conditions of standard animal housing [101,101—103]. In contrast to our findings and the other data noted above that implicate various whole-body ADAM17 mutants in hypermetabolism [38], Lownik and colleagues observed that deletion of ADAM17 in adipose tissues had little impact on whole-body metabolism and inflammation in HFD-triggered obesity [104]. One key difference between our studies and theirs is the duration of exposure to HFD. Lownik and colleagues assayed their animals after 12—14 weeks, a relatively short period of HFD feeding [104]. By contrast, as humans are exposed to obesogenic diets throughout a substantial proportion of their lives, we selected a more chronic regimen that mimics middle-aged obesity. According to the CDC, the highest prevalence of obesity is among humans aged 40—59 years of age (i.e., middle age) [105,106]. The analogous period of "middle age" in C57BL/6J mice is estimated by the Jackson laboratory to be between 10 and 14 months [107]. Our model of HFD feeding which exposes the mice to HFD for 26 weeks from the age of 6 weeks (e.g. total of 32 weeks/8 months old at the endpoint) may better approximate the human cohort that has the highest prevalence of obesity. The increased energy expenditure exhibited by ADAM17 KOs could be accounted for by several inter-related mechanisms that enhance the adipose tissue beiging and thermogenesis observed in the KO mice (Figure 1H; Figure 2I—J; Fig. 3N-O) and consequently, an enhanced catabolic state consistent with elevated levels of mRNAs associated with lipolysis or beta-oxidation (Fig. 3L-M). Our cellular (Figure 1, Fig. 7) and transcriptomic studies (Fig. 7) support the view that this is an adipocyte-autonomous circuit that represses adipogenesis, lipid uptake and catabolism and thermogenesis (Fig. S6E). However, it will be interesting to determine, in future studies, whether adipocyte ADAM17 can also impinge on sympathetic tone, the sympathetic innervation of adipose tissues, the recruitment/function of adipose tissue-associated immune cells, or indeed upon endocrine cross talk between adipose tissues and other organs (e.g. the brain, liver). Although there is no prior established connection between Sema4B and metabolic regulation, we can make several general inferences concerning how Sema4B could negatively regulate thermogenesis from the biology of other semaphorins. Semaphorins can signal through intracellular kinases such as PKA [108], which are required for β-adrenergic signal transduction (e.g. to regulate lipolysis). However, the functions of semaphorins are not linear and seem to be determined by the tissue microenvironment. Adding to this complexity is the ability of semaphorins to bind not only to their multiple cognate receptors plexins and neuropilins, but also to several other receptors and coreceptors (e.g. CD72, Tim2, integrins, and proteoglycans [94,109—112]). Indeed, several receptor tyrosine kinases (e.g. VEGFR2, ErbB2, and Met) associate with plexins and neuropilins and are transactivated upon semaphorin binding [94]. Aside from acting as ligands, semaphorins can also act as receptors, via a phenomenon known as reverse signaling [94]. Consistent with our earlier observations of elevated thermogenesis and hypermetabolism in ADAM17 KOs (e.g. a context where Sema4B cleavage/secretion is frustrated), our transcriptomic data suggest that cleaved Sema4B could impair thermogenesis in a pleiotropic manner. For example, this includes impinging directly upon thermogenic gene expression, or upon metabolic processes that are required to support thermogenesis (e.g. lipolysis, lipid uptake). Sema4B also negatively impacts on beta-adrenoceptor expression, which would also indirectly dampen thermogenesis. Interestingly, Sema4B also reduced the mRNA levels of the transcription factors C/ebpα and Pparγ which play crucial roles in (brown) adipocyte differentiation [113,114]. Aside from repressing genes involved in lipolysis, Sema4B seems to negatively impact upon all steps involved in lipid uptake until their breakdown into energy substrates to fuel heat generation by brown adipocytes. Semaphorins act, in part, by regulating the activation state of GTPases [94]. Guanine nucleotide exchange proteins (GEFs) keep GTPases turned on by promoting their binding to GTP while GTPase-activating proteins (GAPs) promote the binding of GTPase to GDP [115]. Interestingly, plexin receptors have a conserved GAP homology domain that activates the GTPase activity of the Rap and Ras family of GTPases [116]. Speculatively, in the context of adipocytes, plexin activation by Sema4b could increase the GAP activity of the G-proteins associated with β-ARs, maintaining the G-proteins in an inactive state. This would dampen downstream signal transduction in response to NE, lipolysis and UCP1 activation. Future studies are needed to address this interesting possibility. In addition to the pronounced negative impact on expression of mRNAs associated with lipid homeostasis and thermogenesis, cleaved Sema4B also promoted the upregulation of extracellular matrix (ECM)-associated genes including transforming growth factor *beta* (Tgf-β), a fibrosis-promoting cytokine [117] and various collagens. Indeed, ADAM17 has an established pro-fibrotic activity [118—120] while pro-fibrotic roles for semaphorins have recently emerged in a variety of disease contexts including in the lung, kidney and the cornea [121—124]. Interestingly, several studies have implicated the aberrant expression of extracellular matrix-associated genes, including collagens, with defective adipose tissue remodeling during obesity [125]. However, evidence for semaphorin-mediated promotion of adipose tissue fibrosis is limited to a single study on Sema3C [126], while the impact of pro-fibrotic genes in adipocyte thermogenesis is still poorly understood [127,128]. Speculatively, cleaved Sema4B

could act on pre-adipocytes or mature adipocytes to promote fibrosis, to trigger a range of negative impacts on adipocyte physiology like on adipose tissue plasticity and insulin resistance [126] or thermogenesis [129]. Our current knowledge on the role of semaphorins in metabolism is very limited and centered on the Sema3 class of semaphorins. To date, the most prominent example that implicates a semaphorin in obesity is on the role of class 3 semaphorins, of which rare variants have been isolated from severely obese human subjects [130]. These semaphorins act upon neuropilin-2 in the hypothalamus to promote the development of melanocortin neuronal circuits that regulate energy homeostasis; loss of neuropilin-2 in pro-opiomelanocortin neurons reduces energy expenditure and promotes weight gain [130]. Moreover, Sema3A is expressed in adipocytes together with neuropilin-1 and is negatively regulated during cold acclimation in BAT [131,132]. In addition, Sema3G has opposing roles in adipogenesis: its plasma levels are increased in obese patients, while its deletion protects mice from HFD-induced weight and fat gain, insulin resistance and glucose tolerance and liver lipogenesis [133,134]. Although our present study identifies a novel adipocyte-autonomous axis for semaphorin signaling in metabolic regulation, it will be interesting to determine whether soluble forms of Sema4B can act hormonally on energy centers in the brain (or indeed, whether shedding of other semaphorins by ADAMs plays a role in energy regulation in the brain). Although the metalloproteases involved in the reported proteolysis of other semaphorins remain to be fully delineated, interestingly, the ectodomains of class 3–7 semaphorins [135–137] or their receptors [138,139] can be cleaved by ADAMs or other metalloproteases. Sema3C for example was shown to be cleaved by ADAMTS1 [140], while Sema3A signaling is regulated by the proteolysis of neuropilin-1 by ADAM17 and ADAM10 [138]. We have shown here that Sema4B shedding is ADAM17-dependent and stimulable by β-AR activation (Figure 5A–E). Like other ADAM17 substrates (and shed metalloprotease substrates more generally) [141,142], we see evidence in HEK cells and in primary adipocytes for additional, ADAM17-independent Sema4B proteolytic activities (Figure 5F). A similar phenomenon has been reported for well-established ADAM17 substrates such as EGFR ligands, which can undergo ADAM17-independent shedding in response to calcium ionophores and calmodulin inhibitors [141]. Future studies will be required to reveal the additional protease(s) responsible for Sema4B shedding, to establish the context within which ADAM17, versus other sheddases, cleave Sema4B, and to dissect whether differentially cleaved forms of Sema4B can elicit different signaling outcomes. ADAM17 is a pleiotropic enzyme crucial for the development and progression of numerous diseases. As targeting ADAM17 has been demonstrated to cause toxicity because of its pleiotropic activity and because of the cross-reactivity of ADAM17 inhibitors with similar metalloproteases [143,144], finding new targets for specific branches of ADAM17 biology is an imperative for the development of novel ADAM17 associated therapies. Therefore, as a novel ADAM17-shed adipokine, Semaphorin 4B could be a promising candidate for the development of new therapeutic strategies to treat obesity.

5. CONCLUSIONS

Our work establishes an important role for ADAM17, through the shedding of the novel adipokine Sema4B as a negative regulator of adipogenesis and thermogenesis that is regulated by beta-adrenoceptor signalling.

DATA AVAILABILITY

Data from the RNAseq experiment have been uploaded to GEO

ACKNOWLEDGEMENTS

The authors thank the anonymous reviewers whose insightful and constructive critiques have helped to improve our manuscript. We thank the Ethics Committee, Animal Facility, Histopathology and Flow cytometry units and the Antibody Service of the Instituto Gulbenkian de Ciência. We thank Hana Dvořáková and Zuzana Vaitová for assistance with production of recombinant Semaphorin 4B. We thank Andreas Püschel for the Sema4b expression plasmid. We acknowledge the support of Fundação Calouste Gulbenkian; Queen's University Belfast; Worldwide Cancer Research (14–1289); a Marie Curie Career Integration Grant (project no. 618769); Fundação para a Ciência e Tecnologica (FCT) grants, SFRH/BCC/52507/2014, PTDC/BEX-BCM/3015/2014 and LISBOA-01–0145-FEDER-031330), funding from 'La Caixa' Foundation under the agreement < LCF/PR/HR17/52150018>; support from the ERDF/ESF project ChemBioDrug (No. CZ.02.1.01/0.0/0.0/16_019/0000729) and by the Deutsche Forschungsgemeinschaft (DFG, German Research Foundation) under Germany's Excellence Strategy within the framework of the Munich Cluster for Systems Neurology (EXC 2145 SyNergy–ID 390857198). This work was developed with the support of the research infrastructure Congento, project LISBOA-01–0145-FEDER-022170, co-financed by Lisboa Regional Operational Programme (Lisboa 2020), under the Portugal 2020 Partnership Agreement, through the European Regional Development Fund (ERDF), and Foundation for Science and Technology (Portugal). This study was supported by research grants from the Government of Catalonia, Spain (SGR 2021/01263) and of the *Instituto de Salud Carlos III* (ISCIII) through the projects PI18/01022 and PI21/01361 (Cofounded by European Regional Development Fund (ERDF) "a way to build Europe" and by the European Social Fund (ESF), "investing in your future"), by the *Fondo Europeo de Desarrollo Regional* (FEDER), and the CIBER *de la Fisiopatología de la Obesidad y la Nutrición* (CIBEROBN), also an initiative ISCIII. We want to acknowledge the kind collaboration of all of the participants involved in this study, the FATBANK platform (also promoted by the CIBEROBN), and the *Biobanc* (B.0000872) of the *Institut d'Investigació Biomèdica de Girona* (IDIBGI), integrated in the Spanish National Biobanks Network. FJO (MS19/00109) is recipient of the Miguel Servet scheme; *Ministerio de Ciencia, Innovación y Universidades, Gobierno de España* (ES).

DECLARATION OF COMPETING INTEREST

The authors declare that they have no known competing financial interests or personal relationships that could have appeared to influence the work reported in this paper.

APPENDIX A. SUPPLEMENTARY DATA

Supplementary data to this article can be found online at https://doi.org/10.1016/j.molmet.2023.101731.

REFERENCES

[1] White CL, Purpera MN, Ballard K, Morrison CD. Decreased food intake following overfeeding involves leptin-dependent and leptin-independent mechanisms. Physiol Behav 2010;100(4):408–16.

[2] Ravussin Y, Edwin E, Gallop M, Xu L, Bartolomé A, Kraakman MJ, et al. Evidence for a non-leptin system that defends against weight gain in overfeeding. Cell Metabol 2018;28(2):289–299.e5.

[3] Richards P, Thornberry NA, Pinto S. The gut-brain axis: identifying new therapeutic approaches for type 2 diabetes, obesity, and related disorders. Mol Metabol 2021;46:101175.

[4] Müller TD, Blüher M, Tschöp MH, DiMarchi RD. Anti-obesity drug discovery: advances and challenges. Nat Rev Drug Discov 2021:1–23.

[5] Loos RJF, Yeo GSH. The genetics of obesity: from discovery to biology. Nat Rev Genet 2022;23(2):120–33.

[6] Harvey I, Boudreau A, Stephens JM. Adipose tissue in health and disease. Open Biol 2020;10(12):200291.

[7] Zwick RK, Guerrero-Juarez CF, Horsley V, Plikus MV. Anatomical, physiological, and functional diversity of adipose tissue. Cell Metabol 2018;27(1):68–83.

[8] Desruisseaux MS, Nagajyothi, Trujillo ME, Tanowitz HB, Scherer PE. Adipocyte, adipose tissue, and infectious disease. Infect Immun 2007;75(3):1066–78.

[9] Scheja L, Heeren J. The endocrine function of adipose tissues in health and cardiometabolic disease. Nat Rev Endocrinol 2019;15(9):507–24.

[10] Rexford A, Flier JS. Leptin. Annu Rev Physiol 2000;62(7):413–37.

[11] Jequier E. Leptin signaling, adiposity, and energy balance. Ann N Y Acad Sci 2002;967(1):379–88.

[12] Griggio MA, Richard D, Leblanc J. Effects of fasting and food restriction on sympathetic activity in brown adipose tissue in mice. J Comp Physiol B 1992;162(7):602–6.

[13] Kawate R, Talan MI, Engel BT. Sympathetic nervous activity to brown adipose tissue increases in cold-tolerant mice. Physiol Behav 1994;55(5):921–5.

[14] Cypess AM, Chen YC, Sze C, Wang K, English J, Chan O, et al. Cold but not sympathomimetics activates human brown adipose tissue in vivo. Proc Natl Acad Sci U S A 2012;109(25):10001–5.

[15] Bartness TJ, Song CK. Thematic review series: adipocyte biology. Sympathetic and sensory innervation of white adipose tissue. J Lipid Res 2007;48(8):1655–72.

[16] François M, Torres H, Huesing C, Zhang R, Saurage C, Lee N, et al. Sympathetic innervation of the interscapular brown adipose tissue in mouse. Ann N Y Acad Sci 2019;1454(1):3–13.

[17] Münzberg H, Floyd E, Chang JS. Sympathetic innervation of white adipose tissue: to beige or not to beige. Physiology 2021;36(4):246–55.

[18] Duncan RE, Ahmadian M, Jaworski K, Sarkadi-Nagy E, Sul HS. Regulation of lipolysis in adipocytes. Annu Rev Nutr 2007;27:79–101.

[19] Grabner GF, Xie H, Schweiger M, Zechner R. Lipolysis: cellular mechanisms for lipid mobilization from fat stores. Nat Metab 2021;3(11):1445–65.

[20] Collins S. β-Adrenoceptor signaling networks in adipocytes for recruiting stored fat and energy expenditure. Front Endocrinol 2011;2:102.

[21] Cannon B, Nedergaard J. Brown adipose tissue: function and physiological significance. Physiol Rev 2004;84(1):277–359.

[22] Wade G, McGahee A, Ntambi JM, Simcox J. Lipid transport in Brown adipocyte thermogenesis. Front Physiol 2021;12:787535.

[23] Crichton PG, Lee Y, Kunji ER. The molecular features of uncoupling protein 1 support a conventional mitochondrial carrier-like mechanism. Biochimie 2017;134:35–50.

[24] Fedorenko A, Lishko PV, Kirichok Y. Mechanism of fatty-acid-dependent UCP1 uncoupling in brown fat mitochondria. Cell 2012;151(2):400–13.

[25] Cannon B, Nedergaard J. Nonshivering thermogenesis and its adequate measurement in metabolic studies. J Exp Biol 2011;214(Pt 2):242–53.

[26] Roesler A, Kazak L. UCP1-independent thermogenesis. Biochem J 2020;477(3):709–25.

[27] Wu J, Boström P, Sparks LM, Ye L, Choi JH, Giang AH, et al. Beige adipocytes are a distinct type of thermogenic fat cell in mouse and human. Cell 2012;150(2):366–76.

[28] Petrovic N, Walden TB, Shabalina IG, Timmons JA, Cannon B, Nedergaard J. proliferator-activated receptor γ (PPARγ) activation of epididymally derived white adipocyte cultures reveals a population of thermogenically competent, UCP1-containing adipocytes molecularly distinct from classic brown adipocytes. J Biol Chem 2010;285(10):7153–64.

[29] Cohen P, Kajimura S. The cellular and functional complexity of thermogenic fat. Nat Rev Mol Cell Biol 2021;22(6):393–409.

[30] Ghaben AL, Scherer PE. Adipogenesis and metabolic health. Nat Rev Mol Cell Biol 2019;20(4):242–58.

[31] Singh AM, Zhang L, Avery J, Yin A, Du Y, Wang H, et al. Human beige adipocytes for drug discovery and cell therapy in metabolic diseases. Nat Commun 2020;11(1):2758.

[32] Thyagarajan B, Foster MT. Beiging of white adipose tissue as a therapeutic strategy for weight loss in humans. Horm Mol Biol Clin Invest 2017;31:2. j/hmbci.2017.31.issue-2/hmbci.

[33] Silva GDN, Amato AA. Thermogenic adipose tissue aging: mechanisms and implications. Front Cell Dev Biol 2022;10:955612.

[34] Moss ML, Jin S-LC, Milla ME, Burkhart W, Carter HL, Chen W-J, et al. Cloning of a disintegrin metalloproteinase that processes precursor tumour-necrosis factor-α. Nature 1997;385(6618):733–6.

[35] Black RA, Rauch CT, Kozlosky CJ, Peschon JJ, Slack JL, Wolfson MF, et al. A metalloproteinase disintegrin that releases tumour-necrosis factor-α from cells. Nature 1997;385(6618):729–33.

[36] Zunke F, Rose-John S. The shedding protease ADAM17: physiology and pathophysiology. Biochim Biophys Acta Mol Cell Res 2017;1864(11 Pt B):2059–70.

[37] Schumacher N, Rose-John S. ADAM17 activity and IL-6 trans-signaling in inflammation and cancer. Cancers 2019;11:E1736.

[38] Gelling RW, Yan W, Al-Noori S, Pardini A, Morton GJ, Ogimoto K, et al. Deficiency of TNFalpha converting enzyme (TACE/ADAM17) causes a lean, hypermetabolic phenotype in mice. Endocrinology 2008;149(12):6053–64.

[39] Serino M, Menghini R, Fiorentino L, Amoruso R, Mauriello A, Lauro D, et al. Mice heterozygous for tumor necrosis factor-alpha converting enzyme are protected from obesity-induced insulin resistance and diabetes. Diabetes 2007;56(10):2541–6.

[40] Hotamisligil GS, Shargill NS, Spiegelman BM. Adipose expression of tumor necrosis factor-alpha: direct role in obesity-linked insulin resistance. Science 1993;259(5091):87–91.

[41] Hotamisligil GS. The role of TNFα and TNF receptors in obesity and insulin resistance. J Intern Med 1999;245(6):621–5.

[42] Uysal KT, Wiesbrock SM, Marino MW, Hotamisligil GS. Protection from obesity-induced insulin resistance in mice lacking TNF-α function. Nature 1997;389(6651):610–4.

[43] Badenes M, Amin A, González-García I, Félix I, Burbridge E, Cavadas M, et al. Deletion of iRhom2 protects against diet-induced obesity by increasing thermogenesis. Mol Metabol 2020;31:67–84.

[44] Adrain C, Zettl M, Christova Y, Taylor N, Freeman M. Tumor necrosis factor signaling requires iRhom2 to promote trafficking and activation of TACE. Science 2012;335(6065):225–8.

[45] McIlwain DR, Lang PA, Maretzky T, Hamada K, Ohishi K, Maney SK, et al. iRhom2 regulation of TACE controls TNF-mediated protection against Listeria and responses to LPS. Science 2012;335(6065):229–32.

[46] Maretzky T, McIlwain DR, Issuree PD, Li X, Malapeira J, Amin S, et al. iRhom2 controls the substrate selectivity of stimulated ADAM17-dependent ectodomain shedding. Proc Natl Acad Sci U S A 2013;110(28):11433–8.

[47] Cavadas M, Oikonomidi I, Gaspar CJ, Burbridge E, Badenes M, Félix I, et al. Phosphorylation of iRhom2 controls stimulated proteolytic shedding by the metalloprotease ADAM17/TACE. Cell Rep 2017;21(3):745–57.

[48] Grieve AG, Xu H, Künzel U, Bambrough P, Sieber B, Freeman M. Phosphorylation of iRhom2 at the plasma membrane controls mammalian TACE-dependent inflammatory and growth factor signalling. Elife 2017;6:e23968.

[49] Oikonomidi I, Burbridge E, Cavadas M, Sullivan G, Collis B, Naegele H, et al. iTAP, a novel iRhom interactor, controls TNF secretion by policing the stability of iRhom/TACE. Elife 2018;7:e35032.

[50] Künzel U, Grieve AG, Meng Y, Sieber B, Cowley SA, Freeman M. FRMD8 promotes inflammatory and growth factor signalling by stabilising the iRhom/ADAM17 sheddase complex. Elife 2018;7:e35012.
[51] Badenes M, Burbridge E, Oikonomidi I, Amin A, de Carvalho É, Kosack L, et al. The ADAM17 sheddase complex regulator iTAP modulates inflammation, epithelial repair, and tumor growth. 2022.
[52] Westerterp KR. Diet induced thermogenesis. Nutr Metab 2004;1:5.
[53] Saito M, Matsushita M, Yoneshiro T, Okamatsu-Ogura Y. Brown adipose tissue, diet-induced thermogenesis, and thermogenic food ingredients: from mice to men. Front Endocrinol 2020;11:222.
[54] Fischer AW, Schlein C, Cannon B, Heeren J, Nedergaard J. Intact innervation is essential for diet-induced recruitment of brown adipose tissue. Am J Physiol Endocrinol Metab 2019;316(3):E487–503.
[55] Prenzel N, Zwick E, Daub H, Leserer M, Abraham R, Wallasch C, et al. EGF receptor transactivation by G-protein-coupled receptors requires metalloproteinase cleavage of proHB-EGF. Nature 1999;402(6764):884–8.
[56] Gooz M, Gooz P, Luttrell LM, Raymond JR. 5-HT2A receptor induces ERK phosphorylation and proliferation through ADAM-17 tumor necrosis factor-α-converting enzyme (TACE) activation and heparin-bound epidermal growth factor-like growth factor (HB-EGF) shedding in mesangial cells. J Biol Chem 2006;281(30):21004–12.
[57] Yin J, Yu FS. ERK1/2 mediate wounding- and G-protein-coupled receptor ligands-induced EGFR activation via regulating ADAM17 and HB-EGF shedding. Invest Ophthalmol Vis Sci 2009;50(1):132–9.
[58] Horiuchi K, Kimura T, Miyamoto T, Takaishi H, Okada Y, Toyama Y, et al. Cutting edge: TNF-alpha-converting enzyme (TACE/ADAM17) inactivation in mouse myeloid cells prevents lethality from endotoxin shock. J Immunol 2007;179(5):2686–9.
[59] Eguchi J, Wang X, Yu S, Kershaw EE, Chiu PC, Dushay J, et al. Transcriptional control of adipose lipid handling by IRF4. Cell Metabol 2011;13(3):249–59.
[60] Carobbio S, Guenantin AC, Bahri M, Rodriguez-Fdez S, Honig F, Kamzolas I, et al. Unraveling the developmental roadmap toward human Brown AdipoSeTissue. Stem Cell Rep 2021;16(4):1010.
[61] Tran KV, Brown EL, DeSouza T, Jespersen NZ, Nandrup-Bus C, Yang Q, et al. Human thermogenic adipocyte regulation by the long noncoding RNA LINC00473. Nat Metab 2020;2(5):397–412.
[62] Tüshaus J, Müller SA, Kataka ES, Zaucha J, Sebastian Monasor L, Su M, et al. An optimized quantitative proteomics method establishes the cell type-resolved mouse brain secretome. EMBO J 2020;39(20):e105693.
[63] Tüshaus J, Müller SA, Shrouder J, Arends M, Simons M, Plesnila N, et al. The pseudoprotease iRhom1 controls ectodomain shedding of membrane proteins in the nervous system. Faseb J 2021;35(11):e21962.
[64] Burkhardt C, Müller M, Badde A, Garner CC, Gundelfinger ED, Püschel AW. Semaphorin 4B interacts with the post-synaptic density protein PSD-95/SAP90 and is recruited to synapses through a C-terminal PDZ-binding motif. FEBS Lett 2005;579(17):3821–8.
[65] Adrain C, Strisovsky K, Zettl M, Hu L, Lemberg MK, Freeman M. Mammalian EGF receptor activation by the rhomboid protease RHBDL2. EMBO Rep 2011;12(5):421–7.
[66] Naviaux RK, Costanzi E, Haas M, Verma IM. The pCL vector system: rapid production of helper-free, high-titer, recombinant retroviruses. J Virol 1996;70(8):5701–5.
[67] Cavadas M, Oikonomidi I, Gaspar CJ, Burbridge E, Badenes M, Félix I, et al. Phosphorylation of iRhom2 controls stimulated proteolytic shedding by the metalloprotease ADAM17/TACE. Cell Rep 2017;21(3):745–57.
[68] Klein J, Fasshauer M, Ito M, Lowell BB, Benito M, Kahn CR. β3-Adrenergic stimulation differentially inhibits insulin signaling and decreases insulin-induced glucose uptake in brown adipocytes. J Biol Chem 1999;274(49):34795–802.
[69] Picelli S, Faridani OR, Björklund AK, Winberg G, Sagasser S, Sandberg R. Full-length RNA-seq from single cells using Smart-seq2. Nat Protoc 2014;9(1):171–81.
[70] Baym M, Kryazhimskiy S, Lieberman TD, Chung H, Desai MM, Kishony R. Inexpensive multiplexed library preparation for megabase-sized genomes. PLoS One 2015;10(5):e0128036.
[71] Dobin A, Davis CA, Schlesinger F, Drenkow J, Zaleski C, Jha S, et al. STAR: ultrafast universal RNA-seq aligner. Bioinformatics 2013;29(1):15–21.
[72] Anders S, Pyl PT, Huber W. HTSeq–a Python framework to work with high-throughput sequencing data. Bioinformatics 2015;31(2):166–9.
[73] Love MI, Huber W, Anders S. Moderated estimation of fold change and dispersion for RNA-seq data with DESeq2. Genome Biol 2014;15(12):550.
[74] Sherman BT, Hao M, Qiu J, Jiao X, Baseler MW, Lane HC, et al. DAVID: a web server for functional enrichment analysis and functional annotation of gene lists (2021 update). Nucleic Acids Res 2022;50(W1):W216–21.
[75] Ortega FJ, Mercader JM, Moreno-Navarrete JM, Nonell L, Puigdecanet E, Rodriquez-Hermosa JI, et al. Surgery-induced weight loss is associated with the downregulation of genes targeted by MicroRNAs in adipose tissue. J Clin Endocrinol Metab 2015;100(11):E1467–76.
[76] Prenzel N, Zwick E, Daub H, Leserer M, Abraham R, Wallasch C, et al. EGF receptor transactivation by G-protein-coupled receptors requires metalloproteinase cleavage of proHB-EGF. Nature 1999;402(6764):884–8.
[77] Palanisamy S, Xue C, Ishiyama S, Naga Prasad SV, Gabrielson K. GPCR-ErbB transactivation pathways and clinical implications. Cell Signal 2021;86:110092.
[78] Collins S. β-Adrenergic receptors and adipose tissue metabolism: evolution of an old story. Annu Rev Physiol 2022;84:1–16.
[79] Shook RP, Hand GA, Paluch AE, Wang X, Moran R, Hébert JR, et al. High respiratory quotient is associated with increases in body weight and fat mass in young adults. Eur J Clin Nutr 2016;70(10):1197–202.
[80] Burke SJ, Batdorf HM, Martin TM, Burk DH, Noland RC, Cooley CR, et al. Liquid sucrose consumption promotes obesity and impairs glucose tolerance without altering circulating insulin levels. Obesity 2018;26(7):1188–96.
[81] Jo J, Gavrilova O, Pack S, Jou W, Mullen S, Sumner AE, et al. Hypertrophy and/or hyperplasia: dynamics of adipose tissue growth. PLoS Comput Biol 2009;5(3):e1000324.
[82] Attie AD, Scherer PE. Adipocyte metabolism and obesity. J Lipid Res 2009;50(Suppl):S395–9.
[83] Geisler CE, Renquist BJ. Hepatic lipid accumulation: cause and consequence of dysregulated glucoregulatory hormones. J Endocrinol 2017;234(1):R1–21.
[84] Koonen DP, Jacobs RL, Febbraio M, Young ME, Soltys CL, Ong H, et al. Increased hepatic CD36 expression contributes to dyslipidemia associated with diet-induced obesity. Diabetes 2007;56(12):2863–71.
[85] Strissel KJ, Stancheva Z, Miyoshi H, Perfield JW, DeFuria J, Jick Z, et al. Adipocyte death, adipose tissue remodeling, and obesity complications. Diabetes 2007;56(12):2910–8.
[86] De Taeye BM, Novitskaya T, McGuinness OP, Gleaves L, Medda M, Covington JW, et al. Macrophage TNF-alpha contributes to insulin resistance and hepatic steatosis in diet-induced obesity. Am J Physiol Endocrinol Metab 2007;293(3):E713–25.
[87] Sugawara K, Schneider MR, Dahlhoff M, Kloepper JE, Paus R. Cutaneous consequences of inhibiting EGF receptor signaling in vivo: normal hair follicle development, but retarded hair cycle induction and inhibition of adipocyte growth in Egfr(Wa5) mice. J Dermatol Sci 2010;57(3):155–61.
[88] Choung S, Kim JM, Joung KH, Lee ES, Kim HJ, Ku BJ. Epidermal growth factor receptor inhibition attenuates non-alcoholic fatty liver disease in diet-induced obese mice. PLoS One 2019;14(2):e0210828.
[89] Timper K, Denson JL, Steculorum SM, Heilinger C, Engström-Ruud L, Wunderlich CM, et al. IL-6 improves energy and glucose homeostasis in obesity via enhanced central IL-6 trans-signaling. Cell Rep 2017;19(2):267–80.

[90] Schöbitz B, Pezeshki G, Pohl T, Hemmann U, Heinrich PC, Holsboer F, et al. Soluble interleukin-6 (IL-6) receptor augments central effects of IL-6 in vivo. Faseb J 1995;9(8):659–64.

[91] Wallenius V, Wallenius K, Ahrén B, Rudling M, Carlsten H, Dickson SL, et al. Interleukin-6-deficient mice develop mature-onset obesity. Nat Med 2002;8(1):75–9.

[92] Wallenius K, Wallenius V, Sunter D, Dickson SL, Jansson J-O. Intracerebroventricular interleukin-6 treatment decreases body fat in rats. Biochem Biophys Res Commun 2002;293(1):560–5.

[93] Tüshaus J, Müller SA, Kataka ES, Zaucha J, Sebastian Monasor L, Su M, et al. An optimized quantitative proteomics method establishes the cell type-resolved mouse brain secretome. EMBO J 2020;39(20):e105693.

[94] Alto LT, Terman JR. Semaphorins and their signaling mechanisms. Semaphorin signaling 2017:1–25.

[95] Ramseyer VD, Granneman JG. Adrenergic regulation of cellular plasticity in brown, beige/brite and white adipose tissues. Adipocyte 2016;5(2):119–29.

[96] Christie SM, Hao J, Tracy E, Buck M, Yu JS, Smith AW. Interactions between semaphorins and plexin-neuropilin receptor complexes in the membranes of live cells. J Biol Chem 2021;297(2):100965.

[97] Kerr AG, Andersson DP, Rydén M, Arner P, Dahlman I. Long-term changes in adipose tissue gene expression following bariatric surgery. J Intern Med 2020;288(2):219–33.

[98] U Din M, Saari T, Raiko J, Kudomi N, Maurer SF, Lahesmaa M, et al. Postprandial oxidative metabolism of human Brown fat indicates thermogenesis. Cell Metabol 2018;28(2):207–216.e3.

[99] Lorenzen I, Lokau J, Korpys Y, Oldefest M, Flynn CM, Künzel U, et al. Control of ADAM17 activity by regulation of its cellular localisation. Sci Rep 2016;6:35067.

[100] Wang Z. Transactivation of epidermal growth factor receptor by G protein-coupled receptors: recent progress, challenges and future research. Int J Mol Sci 2016;17(1):E95.

[101] Fischer AW, Cannon B, Nedergaard J. Optimal housing temperatures for mice to mimic the thermal environment of humans: an experimental study. Mol Metabol 2018;7:161–70.

[102] Škop V, Guo J, Liu N, Xiao C, Hall KD, Gavrilova O, et al. Mouse thermoregulation: introducing the concept of the thermoneutral point. Cell Rep 2020;31(2):107501.

[103] Ravussin Y, LeDuc CA, Watanabe K, Leibel RL. Effects of ambient temperature on adaptive thermogenesis during maintenance of reduced body weight in mice. Am J Physiol Regul Integr Comp Physiol 2012;303(4):R438–48.

[104] Lownik JC, Farrar JS, Pearce JV, Celi FS, Martin RK. Adipocyte ADAM17 plays a limited role in metabolic inflammation. Adipocyte 2020;9(1):509–22.

[105] Boutari C, Mantzoros CS. A 2022 update on the epidemiology of obesity and a call to action: as its twin COVID-19 pandemic appears to be receding, the obesity and dysmetabolism pandemic continues to rage on. Metabolism 2022;133:155217.

[106] Gelfand SD. Nudging, bullshitting, and the meta-nudge. Camb Q Healthc Ethics 2023;32(1):56–68.

[107] Kupferschmidt K. On the trail of bullshit. Science 2022;375(6587):1334–7.

[108] Yang T, Terman JR. 14-3-3ε couples protein kinase A to semaphorin signaling and silences plexin RasGAP-mediated axonal repulsion. Neuron 2012;74(1):108–21.

[109] Kumanogoh A, Watanabe C, Lee I, Wang X, Shi W, Araki H, et al. Identification of CD72 as a lymphocyte receptor for the class IV semaphorin CD100: a novel mechanism for regulating B cell signaling. Immunity 2000;13(5):621–31.

[110] Cho JY, Chak K, Andreone BJ, Wooley JR, Kolodkin AL. The extracellular matrix proteoglycan perlecan facilitates transmembrane semaphorin-mediated repulsive guidance. Genes Dev 2012;26(19):2222–35.

[111] Kumanogoh A, Marukawa S, Suzuki K, Takegahara N, Watanabe C, Ch'ng E, et al. Class IV semaphorin Sema4A enhances T-cell activation and interacts with Tim-2. Nature 2002;419(6907):629–33.

[112] Pasterkamp RJ, Peschon JJ, Spriggs, Kolodkin AL. Semaphorin 7A promotes axon outgrowth through integrins and MAPKs. Nature 2003;424(6947):398–405.

[113] Nedergaard J, Petrovic N, Lindgren EM, Jacobsson A, Cannon B. PPARgamma in the control of brown adipocyte differentiation. Biochim Biophys Acta 2005;1740(2):293–304.

[114] Manchado C, Yubero P, Viñas O, Iglesias R, Villarroya F, Mampel T, et al. CCAAT/enhancer-binding proteins α and β in brown adipose tissue: evidence for a tissue-specific pattern of expression during development. Biochem J 1994;302(3):695–700.

[115] Bos JL, Rehmann H, Wittinghofer A. GEFs and GAPs: critical elements in the control of small G proteins. Cell 2007;129(5):865–77.

[116] Wang Y, He H, Srivastava N, Vikarunnessa S, Chen YB, Jiang J, et al. Plexins are GTPase-activating proteins for Rap and are activated by induced dimerization. Sci Signal 2012;5:207. ra6.

[117] Biernacka A, Dobaczewski M, Frangogiannis NG. TGF-β signaling in fibrosis. Growth Factors 2011;29(5):196–202.

[118] Kefaloyianni E, Muthu ML, Kaeppler J, Sun X, Sabbisetti V, Chalaris A, et al. ADAM17 substrate release in proximal tubule drives kidney fibrosis. JCI Insight 2016;1(13):87023.

[119] Matsui Y, Tomaru U, Miyoshi A, Ito T, Fukaya S, Miyoshi H, et al. Overexpression of TNF-α converting enzyme promotes adipose tissue inflammation and fibrosis induced by high fat diet. Exp Mol Pathol 2014;97(3):354–8.

[120] Wang X, Oka T, Chow FL, Cooper SB, Odenbach J, Lopaschuk GD, et al. Tumor necrosis factor-alpha-converting enzyme is a key regulator of agonist-induced cardiac hypertrophy and fibrosis. Hypertension 2009;54(3):575–82.

[121] Carvalheiro T, Affandi AJ, Malvar-Fernández B, Dullemond I, Cossu M, Ottria A, et al. Induction of inflammation and fibrosis by semaphorin 4A in systemic sclerosis. Arthritis Rheumatol 2019;71(10):1711–22.

[122] Jeon KI, Nehrke K, Huxlin KR. Semaphorin 3A potentiates the profibrotic effects of transforming growth factor-β1 in the cornea. Biochem Biophys Res Commun 2020;521(2):333–9.

[123] Peng HY, Gao W, Chong FR, Liu HY, Zhang JI. Semaphorin 4A enhances lung fibrosis through activation of Akt via PlexinD1 receptor. J Biosci 2015;40(5):855–62.

[124] Sang Y, Tsuji K, Fukushima K, Takahashi K, Kitamura S, Wada J. Semaporin3A inhibitor ameliorates renal fibrosis through the regulation of JNK signaling. Am J Physiol Ren Physiol 2021;321(6):F740–56.

[125] Ruiz-Ojeda FJ, Méndez-Gutiérrez A, Aguilera CM, Plaza-Díaz J. Extracellular matrix remodeling of adipose tissue in obesity and metabolic diseases. Int J Mol Sci 2019;20(19):E4888.

[126] Mejhert N, Wilfling F, Esteve D, Galitzky J, Pellegrinelli V, Kolditz CI, et al. Semaphorin 3C is a novel adipokine linked to extracellular matrix composition. Diabetologia 2013;56(8):1792–801.

[127] Hasegawa Y, Ikeda K, Chen Y, Alba DL, Stifler D, Shinoda K, et al. Repression of adipose tissue fibrosis through a PRDM16-gtf2ird1 complex improves systemic glucose homeostasis. Cell Metabol 2018;27(1):180–194.e6.

[128] Chouchani ET, Kajimura S. Metabolic adaptation and maladaptation in adipose tissue. Nat Metab 2019;1(2):189–200.

[129] Gonzalez Porras MA, Stojkova K, Vaicik MK, Pelowe A, Goddi A, Carmona A, et al. Integrins and extracellular matrix proteins modulate adipocyte thermogenic capacity. Sci Rep 2021;11(1):5442.

[130] van der Klaauw AA, Croizier S, Mendes de Oliveira E, Stadler LKJ, Park S, Kong Y, et al. Human semaphorin 3 variants link melanocortin circuit development and energy balance. Cell 2019;176(4):729–742.e18.

[131] Giordano A, Coppari R, Castellucci M, Cinti S. Sema3a is produced by brown adipocytes and its secretion is reduced following cold acclimation. J Neurocytol 2001;30(1):5–10.

[132] Giordano A, Cesari P, Capparuccia L, Castellucci M, Cinti S. Sema3A and neuropilin-1 expression and distribution in rat white adipose tissue. J Neurocytol 2003;32(4):345–52.

[133] Lu Q, Zhu L. The role of semaphorins in metabolic disorders. Int J Mol Sci 2020;21(16):E5641.
[134] Liu M, Xie S, Liu W, Li J, Li C, Huang W, et al. Mechanism of SEMA3G knockdown-mediated attenuation of high-fat diet-induced obesity. J Endocrinol 2020;244(1):223–36.
[135] Fong KP, Barry C, Tran AN, Traxler EA, Wannemacher KM, Tang HY, et al. Deciphering the human platelet sheddome. Blood 2011;117(1):e15–26.
[136] Motani K, Kosako H. Activation of stimulator of interferon genes (STING) induces ADAM17-mediated shedding of the immune semaphorin SEMA4D. J Biol Chem 2018;293(20):7717–26.
[137] Browne K, Wang W, Liu RQ, Piva M, O'Connor TP. Transmembrane semaphorin5B is proteolytically processed into a repulsive neural guidance cue. J Neurochem 2012;123(1):135–46.
[138] Romi E, Gokhman I, Wong E, Antonovsky N, Ludwig A, Sagi I, et al. ADAM metalloproteases promote a developmental switch in responsiveness to the axonal repellant Sema3A. Nat Commun 2014;5:4058.
[139] Ito T, Bai T, Tanaka T, Yoshida K, Ueyama T, Miyajima M, et al. Estrogen-dependent proteolytic cleavage of semaphorin 4D and plexin-B1 enhances semaphorin 4D-induced apoptosis during postnatal vaginal remodeling in pubescent mice. PLoS One 2014;9(5):e97909.
[140] Esselens C, Malapeira J, Colomé N, Casal C, Rodríguez-Manzaneque JC, Canals F, et al. The cleavage of semaphorin 3C induced by ADAMTS1 promotes cell migration. J Biol Chem 2010;285(4):2463–73.
[141] Horiuchi K, Le Gall S, Schulte M, Yamaguchi T, Reiss K, Murphy G, et al. Substrate selectivity of epidermal growth factor-receptor ligand sheddases and their regulation by phorbol esters and calcium influx. Mol Biol Cell 2007;18(1):176–88.
[142] Werny L, Grogro A, Bickenbach K, Bülck C, Armbrust F, Koudelka T, et al. MT1-MMP and ADAM10/17 exhibit a remarkable overlap of shedding properties. FEBS J 2023;290(1):93–111.
[143] Murumkar PR, Ghuge RB, Chauhan M, Barot RR, Sorathiya S, Choudhary KM, et al. Recent developments and strategies for the discovery of TACE inhibitors. Expet Opin Drug Discov 2020;15(7):779–801.
[144] Calligaris M, Cuffaro D, Bonelli S, Spanò DP, Rossello A, Nuti E, et al. Strategies to target ADAM17 in disease: from its discovery to the iRhom revolution. Molecules 2021;26(4):944.

